KINETIC EXTINCTION LIMIT OF A SPHERICAL DIFFUSION FLAME ATTACHED TO A BURNER SURFACE

A THESIS SUBMITTED TO THE GRADUATE DIVISION OF THE UNIVERSITY OF HAWAIʻI AT MĀNOA IN PARTIAL FULFILLMENT OF THE REQUIREMENT FOR THE DEGREE OF

MASTER OF SCIENCE

IN

MECHANICAL ENGINEERING

AUGUST 2012

By

Melvin K Rodenhurst III

Thesis Committee:

Dr. Beei-Huan Chao, Chairperson

Dr. Stephen Masutani

Dr. Weilin Qu

Acknowledgements

The funding for this project was made possible by the Renewable Energy and Island Sustainability Program and I am thankful for their support.

I would like to thank Dr. Masutani and Dr. Qu for being committee members. Both have been very supportive and exemplify dedication to their work and their students. I was delighted at how supportive they were of my work and the level of admiration they have for the mechanical engineering discipline. Dr. Masutani has been a great inspiration and was one of the main motivating factors for me pursing mechanical engineering and higher education.

I especially would like to thank Prof. Chao for his guidance and support. He is the epitome of a great mentor. His patience and knowledge of subject matter are unparalleled. Prof. Chao's impressionable teaching methods inspired me to pursue research in the area of thermodynamics and combustion. After working with Prof. Chao for the past four years, I am humbled to have learned a number of life lessons from the perspectives of a great man. I was truly blessed with the opportunity to work for an exemplary advisor and unforgettable role model.

Lastly, there are no words to express how thankful I am to my friends and family for all their unwavering faith and aloha in my aspirations. Mahalo nui loa.

Abstract

In this study the kinetic extinction of diffusion flames at low flow rates was identified. A microgravity burner-stabilized spherical diffusion flame was used to identify the smallest Damköhler number, representing the weakest burning intensity, at which a flame exists. An activation energy asymptotics that split the flow domain to four main regions, namely the core, porous burner, reaction, and outer regions, was used to identify the extinction state. Four limiting flames, based on flow direction and inert distribution, were used to study the effects of various controlling parameters. By reducing the mass flow rate from a flame sufficiently away from the burner, the flame radius is decreased until the flame reaches the burner exit. Further reduction of the flow rate changes the burning to behave like a premixed flame. Results show that for a flame with a constant flow rate, there exists a minimum reaction rate, or Damköhler number, below which steady burning is not possible. For a specific flame with a specified reaction rate, extinction occurs at a higher flow rate, meaning that extinction is easier to occur when the mass diffusion rate (represented by a specified Lewis number) of the burner reactant is higher or when the mass diffusion rate of the ambient reactant is lower. Comparison of the four limiting flames with the same fuel consumption rate reveals that a flame with a smaller mass flow rate is easier to extinguish.

Table of Contents

List of Tables

List of Figures

NOMENCLATURE

$a_{i,j}$	jth order expansion of the integration constants of variable i in the outer regions
B	pre-exponential factor of the reaction
c_i	integration constants
$c_{p,g}$	specific heat of the gas at constant pressure
$c_{p,s}$	specific heat of the solid material used to build the porous burner
D_i	mass diffusion coefficient of species i
Da	Damköhler number of the chemical reaction
E	activation temperature of the chemical reaction
F	fuel
Le_i	Lewis number of species i
m	mass flow rate
O	oxidizer
P	combustion products
q_1	heat of combustion per unit mass of reactant 1 (burner reactant) consumed
q_F	heat of combustion per unit mass of the fuel
r	spatial coordinate along the radial direction
r_i	inner radius of the porous burner
r_b	outer radius of the porous burner
r_f	flame standoff location
T	temperature
T_0	supplied temperature of the gas at the center of the burner
T_b	temperature at the burner exit

T_f flame temperature

T_i temperature at the inner surface of the burner

T_∞ ambient temperature

u radial flow velocity

W_i molecular weight of species i

x_i molar fraction of species i

Y_1 mass fraction of the reactant supplied from the burner

Y_2 mass fraction of the reactant in the ambient

$Y_{1,0}$ supplied value of Y_1 at the center of the burner

$Y_{2,\infty}$ value of Y_2 at the ambient

∞ location of the ambient

Greek Symbols

ε small expansion parameter defined as $\widetilde{T}_f^2 / \widetilde{E}$

θ spatial coordinate along the angular direction

λ_g thermal conductivity of the gas

λ_s thermal conductivity of the solid material used to build the porous burner

$\tilde{\lambda}$ parameter defined as $\varphi + (\lambda_s/\lambda_g)(1 - \varphi)$

ν_i stoichiometric coefficient of species i

Λ reduced Damköhler number of the chemical reaction

ρ_g gas density

ρ_s density of the solid material used to build the porous burner

φ porosity (void space/total space) of the porous burner

ζ stretched spatial variable defined as $(\tilde{r} - \tilde{r}_f)/\varepsilon$

Subscripts

0 supplied values at the center of the burner

1 reactant supplied from the burner

2 reactant in the ambient

b quantities at the outer radius of the burner

F fuel

f quantities at the flame sheet

g properties of the gas

i quantities at the inner radius of the burner

O oxidizer

P combustion products

s properties of the solid material used to build the porous burner

∞ quantities at the ambient

Superscripts

$\sim$ nondimensional quantities

– rescaled quantities

CHAPTER 1

INTRODUCTION

1.1 Importance of Combustion

Before there were high flying airplanes and roaring automobiles, radiantly lit houses, cooking stoves and furnaces, there was simply fire. The advancement of fire is one of the greatest discoveries of building infrastructure throughout the history of the human race, from cooking to the industrial revolution to the modern technologies of today. Without the use of fire, power plants would cease to exist, transportation would be mediocre at best, and the human species would have never made it into outer space. However, the advancement of fire has claimed many lives, due to wild fires and pollutants from power plants and automobiles. Fortunately, there have been significant advances in combustion science since the mid-1970s, which has improved the understanding and control of flames.

Efficient energy utilization in the design and operation of heat and power devices has enabled more efficient and cleaner burning, especially in the cases of internal combustion engines and industrial furnaces. The use of diesel fuel enables saving energy and cost at the refinery stage, due to the advantage of diesel engines being fuel tolerant, unlike the need of highly refined gasoline fuels for gasoline engines. This fuel tolerant application suggests that there is potential in using low-grade or unconventional fuels. The downside is that the diesel engine operates loudly and emits soot and oxides of nitrogen. To reduce the pollutants emitted from the internal combustion engine and other combustion devices, clean burning must be attained [1].

Most of the useable energy comes from burning fossil fuels. Crude oil, being the dominant fossil fuel, is millions of years old. The remains of animals and plants from a marine environment millions of years ago were heated and pressurized by layers and layers of sand and silt, until being converted to crude oil, or petroleum. The word petroleum is derived from the Latin word "petra", meaning rock, and "oleum", meaning oil. This "rock oil" or "oil from the earth" has a higher energy density than coal and other sources of energy, as can be seen in Table 1 [2]. The energy density is the amount of energy per unit mass of a resource. Crude oil has a higher energy density than coal, but is far more expensive to extract and refine. It is obvious that fossil fuels have the potential to produce significantly more energy than, for instance, hardwoods and softwoods [3].

Material	MJ/kg
Hardwoods	16-19
Softwoods	21-23
Charcoal	28-30
Crop Residue	15-19
Dry Straws	17-18
Dried Dung	8-14
Coal	31-33
Peats	6-8
Crude Oil	42-44

Table 1. Energy Density of Materials.

In one barrel of crude oil, there are approximately 10 gallons of diesel, 4 gallons of jet fuel, 19 gallons of gasoline, and 20 gallons of other products, as shown in Figure 1.

In 2009, the U.S. alone consumed 18 million barrels of oil per day [4]. To ensure sufficient supply of the entire energy demand, the use of other fossil fuels, such as coal and natural gas, is required.

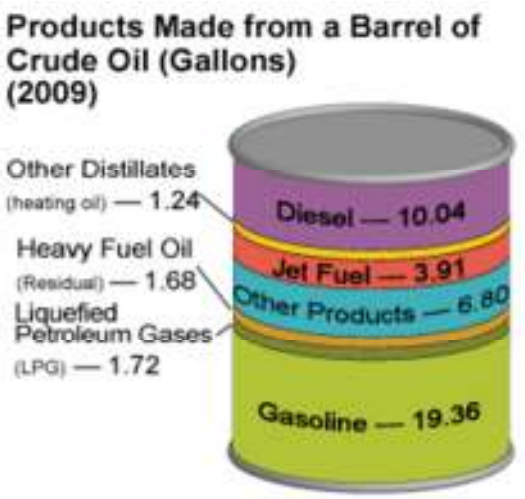

Figure 1. Products Made from a Barrel of Crude Oil.

Harvesting coal is either accomplished by surface or underground mining. Coal can be gasified in air, with or without steam, to produce a combustible gaseous fuel that consists of hydrogen and carbon monoxide. Coal can be made a clean fuel and becomes more desirable with its abundance in supply and high energy density compared to other fuels. Coal has a lower energy density than crude oil, but is less expensive to produce. Burning of crude oil and coal tends to produce soot, sulfur oxides, nitrous oxides, carbon dioxide, unburned hydrocarbons, carbon monoxide, particulate matter, and other byproducts that are harmful to the environment and cause some health issues [1].

When fuel is burned, not all of the reactants are consumed. In the case of fuel lean burning, the fuel in a flame is completely consumed. The excess oxygen remains

unreacted after passing through a flame and is exhausted to the environment. When the burning is fuel rich, the oxygen is completely consumed. The excess fuel is converted to smaller hydrogen and/or carbon containing species through incomplete reaction and can further react with the oxygen in ambient air if the temperature is sufficiently high. For stoichiometric burning, both the fuel and oxygen are completely consumed. Although the supply of the fuel/oxygen mixture can be stoichiometric, stoichiometric burning can never be accomplished because of product dissociation at high temperatures. Combustion devices are then designed to operate under fuel lean conditions, but as close to stoichiometric burning as possible. In engine development, combustion of lean mixtures has the potential of simultaneously increasing the combustion efficiency and reducing the formation of undesired pollutants. Since lean mixtures are hard to ignite, stratified charge combustion is used such that an overall fuel lean mixture is stratified from relatively rich to ultra lean [1].

Environmental quality has made the use of fossil fuels as our primary energy supply a main societal concern. Pollutant production impacts the environment in many ways. In the case of global warming, combustion results in an increased amount of anthropogenic CO_2 in the atmosphere. The production of soot is unsightly and carcinogenic. Sulfur oxides combined with water forms sulfuric acid and precipitates as acid rain, having detrimental effects on aquatic life and causing soil erosion. Moreover, nitrous oxides (NOx) form smog when reacted with unburned hydrocarbons (UHC) and ozone in sunlight which is detrimental to the respiratory system. Indoor pollution from heating devices gives off trace pollutants (CO, NOx, UHC) which may exist at sufficiently high levels that are detrimental to human health. All these pollutants could

be avoided with a higher burning efficiency and a reduction in the pollutant production. It may be argued that renewable energy and other alternative energy sources, such as nuclear, solar, wind, hydroelectric, geothermal, and OTEC could alleviate some of the pollutant problems, but there still exists more pressing concerns [1].

Alternative energy sources only provide a small fraction of the world energy demand, while fossil fuels make up the remaining 85 percent. Production of energy through combustion processes are expected to continue in the foreseeable future, based on the convenience, high-energy density, steady energy supply, and economics associated with burning carbon-based fuels. Advancement in combustion science continues to expand from the previous knowledge to increase burning efficiency and pollutant reduction. Combustion research originated as an empirical method of trial and error through experience and experiments. Today, combustion has grown so much as to being quantitative and even predictive. Applying the research results, combustion related-engineering devices and practices are being incorporated into societies all over the world. Further investigation into combustion science and technologies is made possible by the constant forward progress of mathematical analysis, computational simulation, and experimental techniques. One aspect of combustion that has received a lot of attention is flame extinction [1].

1.2 Impact of Flame Extinction

The practical importance of flame extinction is prevalent in all aspects of combustion. Once a flame is extinguished, there is no heat or energy left to harness.

Flame extinction is known to cause loss of power in engines, operation determent of industrial furnaces, and heating outages in buildings. The more common effects of flame extinction are wasting fuels, generation of pollutants, and fire concerns. Theoretical and experimental studies have shown the importance of flame extinction and have identified the related adverse effects. To gain a better understanding of flame extinction, a few sources should be discussed.

1.3 Extinction of Diffusion Flames

Based on the initial supply of reactants, combustion systems can be divided into premixed and diffusion (nonpremixed) flames. A premixed flame is a flame propagating into a premixed fuel-oxidizer mixture, while a diffusion flame is a flame whose reactants are originally separated and are brought to the flame where mixing and reaction occurs through convection and diffusion transport processes. Extinction of a premixed flame is usually caused by heat loss to the surroundings while a diffusion flame can be extinguished by various mechanisms such as heat loss, hydrodynamic or flame stretch and reactant leakage [1]. Extinction of premixed flame was first analyzed by Spalding [5]. An early notable source that has explored the extinction of diffusion flames extensively is Liñán's seminal paper, where the diffusion-flame, premixed-flame, partial-burning, and ignition regimes of diffusion flames and the flame structures for these regimes and the associated ignition and extinction conditions were identified [6]. The analysis of Liñán had been restricted mainly to laminar counterflow configurations as shown schematically in Figure 2. For this geometry, the oxidizer issues in from the top and the fuel issues in from the bottom to form a stagnation plane in the middle. A

reaction zone, which is the location within the flow domain where chemical reaction takes place, exists near the stagnation plane where the reactants mix and react with each other. It is interesting to note that the results for the reaction-zone structures and extinction can be extended to other configurations by proper modification of some parameters to incorporate different expressions for the residence time [7]. This is because the reaction zone of the flame is thin compared to the transport zones on either side of it as a result of high activation energy for the reaction [6]. A transport zone is a region in which the reactants are brought to the reaction zone through the molecular diffusion and bulk convection processes. Recognizing that most of the practical flames are diffusion flames, this thesis is focused on the extinction of diffusion flames.

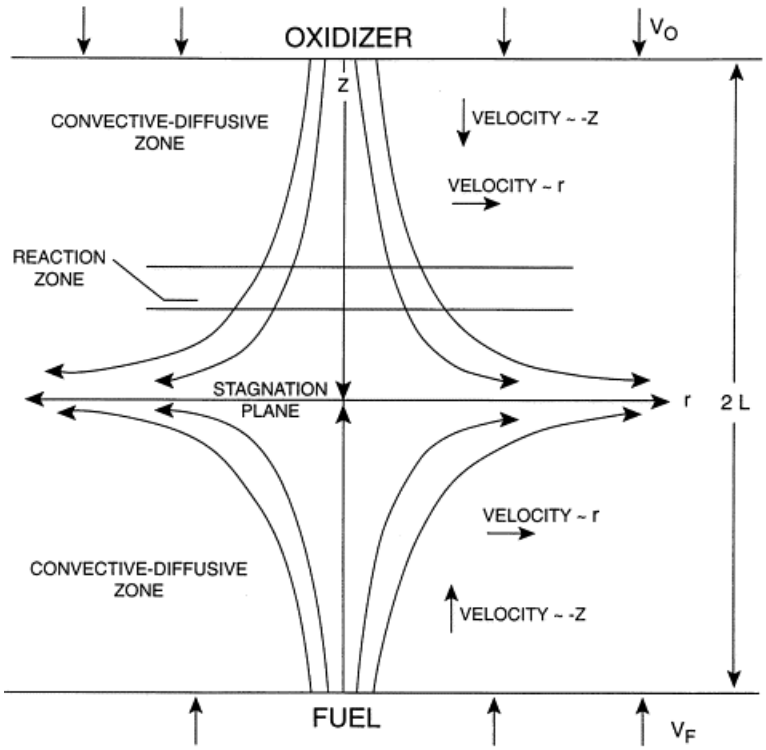

Figure 2. Laminar Counterflow Diffusion Flame.

The structure of a diffusion flame is shown schematically in Figure 3. In the domain of interest, there is a noticeable increase in temperature within the reaction zone where the transport process is reactive-diffusive balanced. The fuel and oxidizer concentrations drastically decrease as they approach the flame and react with each other in the reactive-diffusive zone. The flame extinction is characterized by a Damköhler number, which is the ratio of characteristic flow to reaction times. A high Damköhler number represents a strong flame with a high reaction rate.

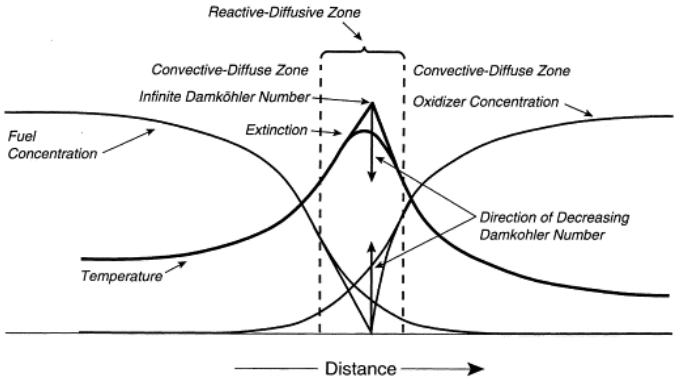

Figure 3. Structure of a Flame.

The S-curve that exhibits the ignition-extinction behavior is shown in Figure 4 in which the maximum temperature is plotted versus Damköhler number. The lower branch where the maximum temperature increases only slightly from the ambient temperature represents the weakly reactive case. By increasing the Damkohler number (reaction rate) from a small value, heat is generated at a higher rate and the temperature is increased. There is a maximum Damköhler number above which a solution does not exist. An additional increase in the Damköhler from this critical value yields the maximum temperature to be jumped to a high value on the upper branch, meaning that the reaction

is transitioned from the weakly reactive condition to vigorous burning and a flame is established. The maximum Damköhler number in the lower branch is then defined as the ignition point. In the upper branch, the reaction is extremely fast, which means that a flame exists, at high Damköhler numbers. Nearly all of the reactants are reacted and a large amount of heat is generated. By reducing the Damköhler number, the reaction rate is decreased and the amount of reactant leakage is increased. As a result, the maximum temperature is dropped. There exists a minimum Damköhler below which a solution does not exist. Additional reduction in the Damköhler number renders the solution be jumped to the lower, weakly reactive reaction and the flame is extinguished. The lowest value of Damköhler number which a flame exists is the extinction state. The middle branch, showing an increase in maximum temperature with decreasing reaction rate, is physically unrealistic. The Damköhler number at ignition is much higher than that at extinction. It was found that by analyzing flamelet structures, the strain or curvature applied to flamelets modifies their internal structure and can lead to flame extinction [8,9,10,11,12].

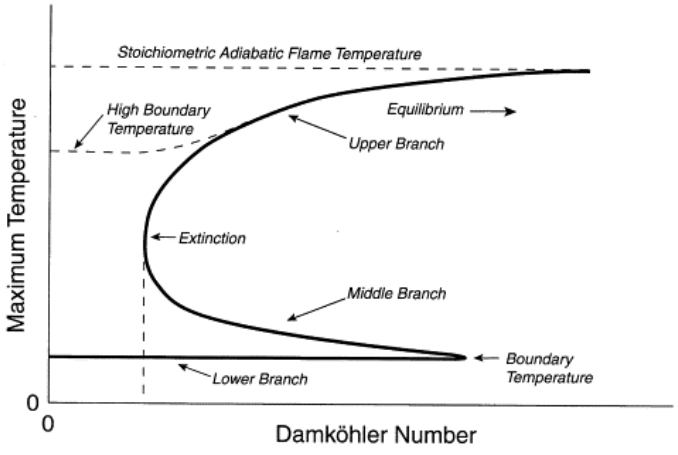

Figure 4. Ignition-Extinction Curve of a Flame.

For a diffusion flame, a number of pollutants are produced when a flame is extinguished. The main pollutants in the fuel side are unreacted hydrocarbons (UHC), polycyclic aromatic hydrocarbons (PAH) and soot, all of which contribute to emissions of particulate matter. The chemical kinetics involved is very complex and depends on a large number of elementary chemical reactions and the formation of a large number of intermediate species. For the production of soot, there are additional chemical processes beyond the formation of PAHs and UHCs, such as particle nucleation, growth, coagulation, agglomeration and oxidation. Another group of pollutants is the production of nitrogen oxides, which is less complicated in the chemical process. Analysis of the flame structure can lead to proper identification of the pollutants. It should be noted that the main flame structure is not altered by the presence of pollutants because they are only present in trace concentrations [10]. However, there are certain species that may have stronger effects on the flame structure and require more detailed analysis in the reaction mechanism.

Flame extinction of counterflow flames has been observed, experimentally, by increasing the exit velocities (the flow velocities at the boundaries shown in Figure 2), thus increasing the strain rate. When the strain rate is increased, the residence time is decreased such that the Damköhler number is decreased. As a consequence, reactants leak through the flame at a higher rate and the flame temperature is reduced. Continuous increase in the strain rate then renders excessive reactant leakage and leads to extinction [10]. The residence time is taken as the time allowed for the flow to pass through the reaction region and is inversely proportional to the flow velocity in the reaction region. This mode of extinction, which occurs at low Damköhler numbers when the reaction rate

is reduced through the reduction of the residence time and can occur without any external loss of heat or reactants, is the kinetic extinction limit. In general, kinetic extinction occurs at low Damköhler numbers, which is caused by high strain rates, high scalar dissipation rates, low reactant concentrations or low mass flow rates, where residence times are low.

When considering radiation, radiant energy loss from the flame can have a significant effect on flame extinction. When a reactive flow with an initial temperature and composition is approaching chemical equilibrium through an adiabatic, isobaric reaction, the maximum temperature is the adiabatic flame temperature. In the presence of radiative heat loss, the maximum flame temperature can fall below the minimum temperature required to support steady burning, causing the flame to extinguish. This extinction limit, which occurs at high Damköhler numbers, is the radiative extinction limit. Using the counterflow flame as an example, the radiative extinction exists at low flow rates (exit velocities). While the reduction of flow rate increases the residence time and the Damlöhler number, which strengthen the reaction, the expansion of the high temperature region intensify the heat loss and reduce the maximum temperature. The negative effect of radiative loss dominates over the increase of residence time by continuously reducing the flow rate and the reaction becomes weaker as the maximum temperature is dropped. The flame is extinguished at a maximum Damköhler number when the heat loss is excessive and the flame can no longer sustain the reaction. Radiative extinction exists only in the presence of radiative heat loss and at high residence times. It is observed experimentally only in microgravity [13] because the

intrusion of buoyancy force reduces the residence time and prevents the extinction condition to be reached.

Existence of the radiative extinction limit was suggested by T'ien [14] in his numerical study and later predicted theoretically by Chao et al. [7] in their analysis of droplet burning. It was later extended to the flame suffering surface radiation [15] and other geometries such as the counterflow flame [16] and the spherical flame stabilized by a porous burner [17,18] One of the more common methods of analyzing flame structure is using counterflow flames. Effects of Lewis number of the reactants, defined as the ratio of thermal diffusivity to the mass diffusivity of the reactant, was also studied [19,20].

1.4 Extinction of Spherical Diffusion Flames

Spherical flames have been extensively adopted to study the burning and extinction of diffusions because of their simplicity in geometry and the experiments can be well controlled. Traditionally, the studies were performed through droplet burning. The kinetic extinction limit of liquid fuel droplets burning in a quiescent oxidizing ambient was first analyzed by Law [21] and the extinction Damköhler number was identified. Applying the result, the minimum droplet size below which the flame cannot exist can be determined. The radiative extinction limit and flammability limit of droplets was later identified by Chao et al. [7]. These studies were performed using activation energy asymptotics with a one-step overall reaction. The existence of radiative extinction was also explored experimentally in microgravity [22,23].

Although droplet burning has been widely adopted to study flame extinction, it is unable to identify the radiative extinction limit because the droplet size only decreases after ignition. Moreover, the flame size is reduced with the droplet such that the burning is quasi-steady, and the flow direction is only flowing from the fuel to the oxidizer. These difficulties can be resolved by adopting a diffusion flame stabilized by a spherical porous burner. In this system, a reactant is supplied from a porous burner and flowing into a large quiescent chamber filled with the other reactant.

A spherical diffusion flame can be established similar to the burning of a fuel droplet except that the flame size can be kept unchanged by keeping the mass flow rate fixed. The flame size can be controlled by varying the mass flow rate of the reactant issued from the burner, and the concentration of the reactants can be controlled by adjusting the type and amount of inert gas supplied with each of the reactants. In addition, the flow direction can be either from the fuel to the oxidizer by issuing a fuel from the burner, or from the oxidizer to the fuel by injecting oxidizer from the burner. To maintain spherical symmetry, experiments must be performed in microgravity. Adopting the burner stabilized flames, Mills and Matalon [18] and Wang and Chao [17] have analyzed and identidied the kinetic and radiative extinction limits of steady diffusion flames. Moreover, Yoo et al. [24] observed from their experimental and numerical studies that the flame might experience oscillatory motion near extinction. Propagation and radiative extinction of transient flames were also studied experimentally and numerically by Tse et al. [25], Santa et al. [13,26] and Tang et al. [27,28], and observed that the extinction behavior of steady and transient flames is different.

1.5 Objectives of the Present Study

The analysis of Wang and Chao [17] revealed that while the radiative extinction limit at high mass flow rates (Large Damköhler numbers or high residence times) always exists for flames that are detached from the burner, the kinetic extinction limit at low mass flow rates are frequently not obtainable because of the intrusion of the burner. To observe the kinetic extinction limit, the flow rate must be sufficiently small for which the flame is located inside of the burner, which is not physically realistic. A recent numerical study by Lecoustre et al. [29] further reveals that after the flame is attached to the burner, additional decrease in the flow rate results in a large amount of the reactant in the ambient to be accumulated in the reaction region and the burning is transitioned from the typical diffusion flame regime to the premixed flame regime as introduced by Liñán [6]. By continually reducing the flow rate, the flame becomes leaner (with respect to the reactant supplied from the burner) and eventually extinguished with insufficient burner reactant.

Burning of a diffusion flame in the premixed flame regime and partial burning regime identified by Liñán [6] has never been experimentally observed before and is considered physically unrealistic because they are located in the middle branch of the S-shaped ignition-extinction curve. Existence of the premixed flame regime requires unusual conditions such as the burner-stabilized flame discussed here. The investigation performed towards this thesis intends to analyze the behavior of this burner-stabilized spherical diffusion flame in the premixed flame regime and understand its extinction characteristics. Based on the flow direction and inert distribution, four limiting flames,

namely the flame with (A) fuel issuing into air, (B) diluted fuel issuing into oxygen, (C) air issuing into fuel and (D) oxygen issuing into diluted fuel have been studied. Effects of Damköhler number (reaction rate), flow rate, residence time and Lewis numbers of the fuel and the oxidizer will be discussed.

The problem definitions and formulation will be shown in Chapter 2. The analysis of the problem using an activation energy asymptotics will be performed in Chapter 3. Results of the study will be discussed in Chapter 4 and the findings will be concluded in Chapter 5.

CHAPTER 2

FORMULATION

2.1 Spherical Porous Burner

The problem of interest is a diffusion flame stabilized by a spherical porous burner, similar to that of Mills and Matalon [18] and Wang and Chao [17]. The burner is considered ideal and gravity is assumed negligible such that the flow is uniform in the radial direction, r. There are two reactants involved in this analysis. Reactant 1 with a given mass flow rate m, temperature of T_0 and mass fraction of $Y_{1,0}$ is supplied from the center of the burner and flowing into an infinite quiescent environment that contains reactant 2 at a temperature of T_∞ and mass fraction of $Y_{2,\infty}$. For a sufficiently high mass flow rate, a flame is established outside of the burner after ignition. The flame, defined as the region in which significant combustion reaction occurs, is spherical and situated near where the stoichiometric reaction between the two reactants is attained. Only small amounts of reactant may leak through the flame for a diffusion flame.

By decreasing the mass flow rate, the flame moves towards the burner and eventually reaches the burner surface. An additional reduction in the flow rate then changes the burning characteristics from the typical diffusion flame to a reaction similar to that of a premixed flame as discussed earlier. Because of the intrusion of the burner, the flame is restrained to stay at the burner exit for all the flow rates below the critical flow rate that just moves the flame to the burner. The reduction of the flow rate reduces the supply of reactant 1 and allows a large amount of reactant 2 to accumulate in the reaction zone and reaches the burner. For this attached flame, the reaction rate is

controlled by the availability of reactant 1 (the lean reactant), as that of a premixed flame. The existence of a large amount of a reactant (reactant 2 for this problem) in a diffusion flame results in a transition from the diffusion flame regime to the premixed flame regime as introduced by Liñán [6].

The flow field is split to four main regions in the analysis, as shown in Figure 5. There is a void core region at the center where the flow ushers in and reactant 1 is supplied; a porous burner region where the flow is stabilized and regulated to yield a uniform flow at the exit; an inner reaction region near the burner exit where the reactants meet and react to produce the combustion products and heat; and an outer region contains reactant 2.

A one-step, overall and irreversible reaction with its rate following a second order Arrhenius kinetics (first order with respect to each of the reactants) with high activation energy is adopted to describe the combustion chemistry. Upon reaching the surface of the porous burner, the inner reactant mixes with the outer reactant, where the flame is ignited.

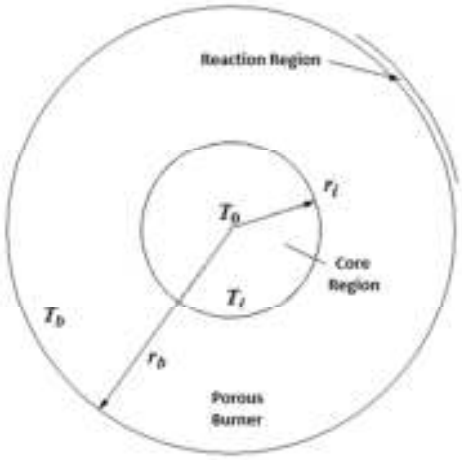

Figure 5. Laminar Counterflow Diffusion Flame.

2.2 Conservation Equations and Boundary Conditions

The reaction is assumed to follow a single step, overall and irreversible reaction between the oxidizer and fuel to produce the product as given by:

$$\nu_F F + \nu_O O \rightarrow \nu_P P \tag{2.1}$$

where F, O and P symbolize the fuel, oxidizer and combustion products, respectively, and ν_F, ν_O and ν_P represent their stoichiometric coefficient. The reaction rate is considered to follow a second order Arrhenius kinetics given by:

$$B\rho_g^2 Y_1 Y_2 \exp(-E/T) \tag{2.2}$$

where B represents the pre-exponential factor of the reaction, ρ_g the gas density, Y_1 the mass fraction of the reactant supplied from the burner, Y_2 the mass fraction of the reactant in the ambient, E the activation temperature of the chemical reaction, and T the temperature. The pre-exponential factor describes the collision frequency between molecules in the reaction. The exponential term in Equation (2.2) accounts for the percentage of successful collisions between molecules. It should be noted that the activation temperature is the ratio of the activation energy to the universal ideal gas constant and is considered, realistically, to be much greater than the maximum flame temperature. Because of the high activation energy, reaction occurs in a thin, reaction region near the burner exit where the maximum flame temperature is located. This will be discussed in Chapter 3.

The flow field and reaction are assumed to be steady and isobaric. The solid and gas are assumed to be in thermal equilibrium within the porous burner, meaning that the temperature of the solid and gas are identical at the same radial distance from the center

of the burner in the burner region. Reactant 1 is issued through the core region at a constant rate given by:

$$m = 4\,\pi r^2\,\rho u \tag{2.3}$$

where m represents the mass flow rate and u the radial flow velocity. The mass flow rate in the porous burner region is similarly given by:

$$m = 4\,\pi r^2\,\rho u\,\varphi \tag{2.4}$$

where φ represents porosity of the burner. The porosity is defined as the fraction of the void space that the flow can pass through. Because the reactant in the ambient cannot penetrate into the burner, there are no chemical reactions in the burner region.

The conservation equations of energy and species in the core region, porous burner region, and gas region external to the burner are:

(a) Core region $(0 < r < r_i)$

$$Y_1 = Y_{1,0} \quad , \quad Y_2 = 0 \quad , \tag{2.5}$$

$$\rho_g u c_{p,g} \frac{dT}{dr} - \frac{1}{r^2}\frac{d}{dr}\left(\lambda_g r^2 \frac{dT}{dr}\right) = 0 \tag{2.6}$$

(b) Within the porous burner $(r_i < r < r_b)$

$$Y_1 = Y_{1,0} \quad , \quad Y_2 = 0 \quad , \tag{2.7}$$

$$\rho_g u c_{p,g} \varphi \frac{dT}{dr} - \frac{1}{r^2}\frac{d}{dr}\left\{[\lambda_g \varphi + \lambda_s (1-\varphi)] r^2 \frac{dT}{dr}\right\} = 0 \tag{2.8}$$

(c) Gas region external of the burner $(r_b < r < \infty)$

$$\rho_g u c_{p,g} \frac{dT}{dr} - \frac{1}{r^2}\frac{d}{dr}\left(\lambda_g r^2 \frac{dT}{dr}\right) = \nu_1 W_1 q_1 B \rho_g^2 Y_1 Y_2 \exp(-E/T) \tag{2.9}$$

$$\rho_g u \frac{dY_1}{dr} - \frac{1}{r^2}\frac{d}{dr}\left(\rho_g D_1 r^2 \frac{dY_1}{dr}\right) = -\nu_1 W_1 B \rho_g^2 Y_1 Y_2 \exp(-E/T) \tag{2.10}$$

$$\rho_g u \frac{dY_2}{dr} - \frac{1}{r^2}\frac{d}{dr}\left(\rho_g D_2 r^2 \frac{dY_2}{dr}\right) = -\nu_2 W_2 B \rho_g^2 Y_1 Y_2 \exp(-E/T) \tag{2.11}$$

where λ_g and λ_s represents the thermal conductivity of the gas and solid material used to build the porous burner, respectively, $c_{p,g}$ the specific heat of the gas at constant pressure, q_1 the heat of combustion per unit mass of reactant 1 consumed, W_i the molecular weight of species i, D_i the mass diffusion coefficient of species i, and r_i and r_b the inner and outer radius of the burner region. Note that since the solid and gas phases are considered in thermal equilibrium, the two energy conservation equations for the gas and solid burner given by:

$$\rho_g u c_{p,g} \frac{dT_g}{dr} - \frac{1}{r^2}\frac{d}{dr}\left(\lambda_g r^2 \frac{dT_g}{dr}\right) = 0 \tag{2.12}$$

$$\frac{1}{r^2}\frac{d}{dr}\left(\lambda_s r^2 \frac{dT_s}{dr}\right) = 0 \tag{2.13}$$

can be combined to obtain Equation (2.8). Equations (2.6) and (2.8) show that there is no reaction inside the porous burner, while Equations (2.9) – (2.11) contain the reaction term.

The boundary and interface conditions for each of the neighboring regions are:

$$r = 0 \ : \quad T = T_0 \quad , \tag{2.14}$$

$$r = r_i \ : \quad T = T_i \quad , \tag{2.15a}$$

$$\lambda_g (dT/dr)_{r_i^-} = [\lambda_g \varphi + \lambda_s (1-\varphi)](dT/dr)_{r_i^+} \quad , \tag{2.15b}$$

$$r = r_b \ : \quad T = T_b \quad , \tag{2.16a}$$

$$[\lambda_g \varphi + \lambda_s (1-\varphi)](dT/dr)_{r_b^-} = \lambda_g (dT/dr)_{r_b^+} \quad , \tag{2.16b}$$

$$\rho_g u Y_1 - (\rho_g D_1)(dY_1/dr) = \rho_g u Y_{1,0} \quad , \tag{2.16c}$$

$$\rho_g u Y_2 - (\rho_g D_2)(dY_2/dr) = 0 \quad , \tag{2.16d}$$

$$r \to \infty \; : \; T \to T_\infty \quad , \quad Y_1 \to 0 \quad , \quad Y_2 \to Y_{2,\infty} \tag{2.17}$$

where T_i and T_b are the temperatures at the inner and outer surface of the porous burner and will be determined later in the analysis. Equations (2.15b) and (2.16b) show the equilibrium of the heat flux in and out of the burner surfaces, while Equations (2.16c) and (2.16d) extend the mass flow rate of the reactants to the burner exit, showing that there is only a mass flow rate of reactant 1 in the burner and there is no penetration of the ambient reaction into the burner.

2.3 Nondimensionalization

The problem to be analyzed can be made nondimensionless by introducing the following nondimensional quantities:

$$\widetilde{T} = \frac{c_{p,g} T}{q_1 Y_{1,0}} \quad , \quad \widetilde{Y}_1 = \frac{Y_1}{Y_{1,0}} \quad , \quad \widetilde{Y}_2 = \frac{\nu_1 W_1}{\nu_2 W_2} \frac{Y_2}{Y_{1,0}} \quad , \quad \widetilde{r} = \frac{r}{r_b} \quad , \quad \widetilde{r}_i = \frac{r_i}{r_b} \quad ,$$

$$\widetilde{E} = \frac{c_{p,g} E}{q_1 Y_{1,0}} \quad , \quad \widetilde{\lambda} = \varphi + (1-\varphi)\frac{\lambda_s}{\lambda_g} \quad , \quad \widetilde{m} = \frac{c_{p,g} m}{4\pi r_b \lambda_g} \quad , \quad \widetilde{\rho}_g = \frac{\rho_g}{\rho_{g,b}} \quad ,$$

$$Da = \frac{\nu_2 W_2 Y_{1,0} c_{p,g} r_b^2 B \rho_b^2}{\lambda_g} \quad , \; Le_i = \frac{\lambda_g / c_{p,g}}{\rho_g D_i}$$

where Y_1 represents the mass fraction of the reactant supplied from the burner, $Y_{1,0}$ the supplied value of Y_1 at the center of the burner, Y_2 the mass fraction of the reactant in the

ambient, $\rho_{g,b}$ the gas density at the burner surface, and ρ_b the density of the porous burner. Applying these nondimensionalized quantities to Equations (2.1) – (2.17), the equations can be nondimensionalized to:

(a) Core region $\left(0 < \tilde{r} < \tilde{r}_i\right)$

$$\tilde{Y}_1 = 1 \quad , \quad \tilde{Y}_2 = 0 \quad , \tag{2.18}$$

$$\frac{d}{d\tilde{r}}\left(\tilde{m}\tilde{T} - \tilde{r}^2 \frac{d\tilde{T}}{d\tilde{r}} \right) = 0 \tag{2.19}$$

(b) Within the porous burner $\left(\tilde{r}_i < \tilde{r} < 1\right)$

$$\tilde{Y}_1 = 1 \quad , \quad \tilde{Y}_2 = 0 \quad , \tag{2.20}$$

$$\frac{d}{d\tilde{r}}\left(\tilde{m}\tilde{T} - \tilde{\lambda}\tilde{r}^2 \frac{d\tilde{T}}{d\tilde{r}} \right) = 0 \tag{2.21}$$

(c) Gas region external of the burner $\left(1 < \tilde{r} < \infty\right)$

$$\frac{1}{\tilde{r}^2}\frac{d}{d\tilde{r}}\left(\tilde{m}\tilde{T} - \tilde{r}^2 \frac{d\tilde{T}}{d\tilde{r}} \right) = Da\tilde{Y}_1\tilde{Y}_2\tilde{\rho}_g^2 \exp(-\tilde{E}/\tilde{T}) \tag{2.22}$$

$$\frac{1}{\tilde{r}^2}\frac{d}{d\tilde{r}}\left(\tilde{m}\tilde{Y}_1 - \frac{\tilde{r}^2}{Le_1}\frac{d\tilde{Y}_1}{d\tilde{r}} \right) = -Da\tilde{Y}_1\tilde{Y}_2\tilde{\rho}_g^2 \exp(-\tilde{E}/\tilde{T}) \tag{2.23}$$

$$\frac{1}{\tilde{r}^2}\frac{d}{d\tilde{r}}\left(\tilde{m}\tilde{Y}_2 - \frac{\tilde{r}^2}{Le_2}\frac{d\tilde{Y}_2}{d\tilde{r}} \right) = -Da\tilde{Y}_1\tilde{Y}_2\tilde{\rho}_g^2 \exp(-\tilde{E}/\tilde{T}) \tag{2.24}$$

(d) Boundary and interface conditions

$$\tilde{r} = 0 \quad : \quad \tilde{T} = \tilde{T}_0 \tag{2.25}$$

$$\tilde{r} = \tilde{r}_i \quad : \quad \tilde{T} = \tilde{T}_i \tag{2.26a}$$

$$(d\tilde{T}/d\tilde{r})_{\tilde{r}_i^-} = \tilde{\lambda}(d\tilde{T}/d\tilde{r})_{\tilde{r}_i^+} \tag{2.26b}$$

$$\widetilde{r} = 1 \quad : \quad \widetilde{T} = \widetilde{T}_b \tag{2.27a}$$

$$\widetilde{\lambda}(d\widetilde{T} / d\widetilde{r})_{1^-} = (d\widetilde{T} / d\widetilde{r})_{1^+} \tag{2.27b}$$

$$\widetilde{m}\widetilde{Y}_1 - \frac{\widetilde{r}^2}{Le_1}\frac{d\widetilde{Y}_1}{d\widetilde{r}} = \widetilde{m} \tag{2.27c}$$

$$\widetilde{m}\widetilde{Y}_2 - \frac{\widetilde{r}^2}{Le_2}\frac{d\widetilde{Y}_2}{d\widetilde{r}} = 0 \tag{2.27d}$$

$$\widetilde{r} \to \infty \quad : \quad \widetilde{T} \to \widetilde{T}_\infty \quad , \quad \widetilde{Y}_1 \to 0 \quad , \quad \widetilde{Y}_2 \to \widetilde{Y}_{2,\infty} \tag{2.28}$$

In the dimensionless form, the flame and the surface of the porous burner are at the same radius of 1 in Equation (2.27a), (2.27b), (2.27c), and (2.28d).

CHAPTER 3

ASYMPTOTIC SOLUTION

3.1 Solutions of Temperature in the Core and Within the Porous Burner Regions

In the core region, integrating Equation (2.19) gives:

$$\left(\widetilde{m}\widetilde{T} - \widetilde{r}^{2}\frac{d\widetilde{T}}{d\widetilde{r}} \right) = \mathrm{c} \tag{3.1}$$

Rearranging terms and integrating Equation (3.1) yields:

$$\widetilde{T} = c_1 + c_2 \exp(-\widetilde{m}/\widetilde{r}) \tag{3.2}$$

The integrating constants in Equation (3.2) can be determined by the boundary conditions, expressed in Equations (2.25) and (2.26a). Substitution of the solution back to Equation (3.2) results in:

$$\widetilde{T} = \widetilde{T}_0 + (\widetilde{T}_i - \widetilde{T}_0)\exp[\widetilde{m}(\widetilde{r}_i^{-1} - \widetilde{r}^{-1})] \tag{3.3}$$

Similarly, within the porous burner, integrating Equation (2.21) results in:

$$\widetilde{T} = c_1 + c_2 \exp[-\widetilde{m}/(\widetilde{\lambda}\widetilde{r})] \tag{3.4}$$

Applying the boundary conditions given by Equations (2.26a) and (2.27a), the integration constants in Equation (3.4) can be determined to yield the solution:

$$\widetilde{T} = \widetilde{T}_i + (\widetilde{T}_b - \widetilde{T}_i)\frac{\exp[-\widetilde{m}/(\widetilde{\lambda}\widetilde{r})] - \exp[-\widetilde{m}/(\widetilde{\lambda}\widetilde{r}_i)]}{\exp(-\widetilde{m}/\widetilde{\lambda}) - \exp[-\widetilde{m}/(\widetilde{\lambda}\widetilde{r}_i)]} \tag{3.5}$$

The temperature at the inner surface of the burner, T_i, can be solved, in terms of T_b, by substituting Equations (3.3) and (3.5) to Equation (2.26b). Adopting the solution of T_i, Equation (3.5) can be re-expressed by:

$$\widetilde{T} = \widetilde{T}_0 + (\widetilde{T}_b - \widetilde{T}_0)\exp[(\widetilde{m}/\widetilde{\lambda})(1 - \widetilde{r}^{-1})] \tag{3.6}$$

The value of T_b and the remaining conservations equations in the gas region external of the burner will be solved by activation energy asymptotics.

3.2 High Activation Energy Reaction

For a typical diffusion flame in the limit of infinitely large activation energy, combustion reaction is possible only when the reaction rate is also infinitely large (Damköhler number is infinite). Under these conditions, reaction occurs on an infinitely thin sheet called a reaction sheet or flame sheet. Both of the reactants are completely consumed at the reaction sheet. When the activation energy is high, but finite, reaction is sensitive to temperature variations. Chemical reaction is possible for large, but finite Damköhler numbers, and occurs in a thin, reaction region that envelops the flame sheet, where the maximum temperature is attained. Because of the broadening of the reaction region and the finite reaction rate, a small amount of reactants may leak through the flame without being reacted. For the burning of hydrocarbon fuels in air, the typical overall activation energy is between 30 to 50 kcal/mole. This translates to the activation temperature of 15,000 – 25,000 K, which is much higher than the typical adiabatic flame temperature of 2,000 – 2,500 K and the reaction can be considered to have high activation energy.

On each side of the flame (reaction region), there is a much broader transport region, or so-called preheat region, in which the reactants are transported to the flame by convection and diffusion processes. In the preheat regions, as the reactants approach the flame where heat is generated, they are heated up by the heat transfer from the flame.

The reactants are then entering the reaction region with temperatures close to the maximum temperature, mixed in the molecular level, and react for heat generation. The reaction region may be viewed as a sink for the reactants and a source of heat [1].

For the flame that is attached to the burner as analyzed in this study, the thin reaction region is attached to the burner and there is only one preheat region between the flame and the ambient. The concentration of burner reactant is low in the reaction region and, as mentioned earlier, there is a large amount of ambient reactant in the flame region. The rate of reaction, as a consequence, is dominated by the availability of the burner reactant.

In the analysis, a small parameter, ε, is used to represent the relation between the characteristic length scales of the reaction and preheat zones. Because the difference between these two length scales is a result of high activation energy reaction, the expression of ε depends on the activation energy and will be defined later. By considering the length scale of the preheat zone to be an order of unity quantity, the length scale of the reaction zone is order of ε.

3.3 Outer Solutions in the Gas Region

In the outer region, chemical reaction is negligible because of the low gas temperature. Thus, the conservation Equations (2.22) – (2.24) in the gas region external to the burner do not have a reaction term and are reduced to:

$$\frac{d}{d\tilde{r}}\left(\tilde{m}\tilde{T}^{+}-\tilde{r}^{2}\frac{d\tilde{T}^{+}}{d\tilde{r}}\right)=\frac{d}{d\tilde{r}}\left(\tilde{m}\tilde{Y}_{1}^{+}-\frac{\tilde{r}^{2}}{Le_{1}}\frac{d\tilde{Y}_{1}^{+}}{d\tilde{r}}\right)=\frac{d}{d\tilde{r}}\left(\tilde{m}\tilde{Y}_{2}^{+}-\frac{\tilde{r}^{2}}{Le_{2}}\frac{d\tilde{Y}_{2}^{+}}{d\tilde{r}}\right)=0 \qquad (3.7)$$

The "+" represents the solution of temperature and species concentrations in this region. The only boundary conditions that can be applied to the outer solutions are the ones at ∞ given by Equation (2.28), and are modified to:

$$\widetilde{r} \to \infty \quad : \quad \widetilde{T}^{+} \to \widetilde{T}_{\infty} \quad , \quad \widetilde{Y}_{1}^{+} \to 0 \quad , \quad \widetilde{Y}_{2}^{+} \to \widetilde{Y}_{2,\infty} \tag{3.8}$$

Although the flow field is chemically inert in the O(1) outer region, the outer solutions are affected by the existence of the O(ε) reaction zone. The solutions are required to expand in terms of the small expansion parameter, ε, as:

$$\widetilde{T}^{+} = \widetilde{T}_{0}^{+} + \varepsilon \widetilde{T}_{1}^{+} + O(\varepsilon^{2}) \quad , \tag{3.9}$$

$$\widetilde{Y}_{1}^{+} = \widetilde{Y}_{1,0}^{+} + \varepsilon \widetilde{Y}_{1,1}^{+} + O(\varepsilon^{2}) \quad , \tag{3.10}$$

$$\widetilde{Y}_{2}^{+} = \widetilde{Y}_{2,0}^{+} + \varepsilon \widetilde{Y}_{2,1}^{+} + O(\varepsilon^{2}) \quad , \tag{3.11}$$

Substituting Equations (3.9) – (3.11) to the three expressions of Equation (3.7), expanding the terms in terms of ε, integrating the resulting equations and applying the boundary conditions in Equation (3.8), the equations are defined as:

$$\widetilde{T}_{0}^{+} = \widetilde{T}_{\infty} + a_{T,0}^{+}[1 - \exp(-\widetilde{m} / \widetilde{r})] \quad , \tag{3.12}$$

$$\widetilde{T}_{1}^{+} = -a_{T,1}^{+}[1 - \exp(-\widetilde{m} / \widetilde{r})] \quad , \tag{3.13}$$

$$\widetilde{Y}_{1,0}^{+} = a_{1,0}^{+}[1 - \exp(-\widetilde{m} Le_{1} / \widetilde{r})] \quad , \tag{3.14}$$

$$\widetilde{Y}_{1,1}^{+} = a_{1,1}^{+}[1 - \exp(-\widetilde{m} Le_{1} / \widetilde{r})] \quad , \tag{3.15}$$

$$\widetilde{Y}_{2,0}^{+} = \widetilde{Y}_{2,\infty} - a_{2,0}^{+}[1 - \exp(-\widetilde{m} Le_{2} / \widetilde{r})] \quad , \tag{3.16}$$

$$\widetilde{Y}_{2,1}^{+} = -a_{2,1}^{+}[1 - \exp(-\widetilde{m} Le_{2} / \widetilde{r})] \tag{3.17}$$

where a^+ represents undetermined integration constants. These constants will be determined along with the solutions in the reaction region.

3.4 Expansion of Energy Equation in Reaction Region

For this analysis, the reaction region is attached to the burner such that it is located at $\tilde{r} = 1$ to the leading order. That is, the flame is located at $\tilde{r} = 1$ in the flame sheet limit. To analyze the flame structure in the O(ε) reaction region, a stretch variable is defined as:

$$\zeta = (\tilde{r} - 1)/\varepsilon \tag{3.18}$$

such that the region is expanded to an O(1) domain in the ζ coordinate. Recognizing that only O(ε) variations in the variables are allowed in the O(ε) reaction region, the variables are expanded in terms of ε as:

$$\tilde{T} = \tilde{T}_f - \varepsilon\theta_1 - \varepsilon^2\theta_2 + O(\varepsilon^3) \tag{3.19}$$

$$\tilde{Y}_1 = \varepsilon\phi_1 + \varepsilon^2\phi_2 + O(\varepsilon^3) \quad , \tag{3.20}$$

$$\tilde{Y}_2 = \psi_0 + \varepsilon\psi_1 + \varepsilon^2\psi_2 + O(\varepsilon^3) \tag{3.21}$$

$$\tilde{\rho} = 1 + O(\varepsilon) \tag{3.22}$$

As mentioned before, for this problem, there is a significant amount of the ambient reactant present in the reaction region and its concentration is an O(1) quantity as shown in Equation (3.21). The Arrhenius term in Equation (2.22) can be expanded by substituting in the temperature expansion of Equation (3.19) to yield:

$$\exp(-\tilde{E}/T) = \exp(-\tilde{E}/\tilde{T}_f)\exp(-\theta_1)\{1 + \varepsilon[\theta_2 + \theta_1^2/\tilde{T}_f + O(\varepsilon)] + \cdots\} \tag{3.23}$$

To obtain Equation (2.27), the small expansion parameter is defined as:

$$\varepsilon = \widetilde{T}_f^{\,2} / \widetilde{E} \tag{3.24}$$

where T_f represents the leading order flame temperature, which is the flame temperature in the flame sheet limit. It should be noted that this expression is used for simplicity in the analysis. The value of ε can be defined as any O(1) constant divided by $\tilde{E}$. Substituting the expansions defined in Equations (3.19) – (3.23) to Equation (2.22), expanding the resulting equation in terms of ε, and keeping the leading order terms, we obtain the energy conservation equation, given by:

$$d^2\theta_1 / d\zeta^2 = \Lambda\phi_1 \exp(-\theta_1) \tag{3.25}$$

where Λ is the reduced Damköhler number of the reaction defined as:

$$\Lambda = \varepsilon^2 Da\psi_0 \exp(-\widetilde{E} / \widetilde{T}_f) \tag{3.26}$$

Understanding that the combustion reaction must be important in the reaction region, Λ is defined such that the nonlinear reaction term is balanced with the diffusion (conduction) term in the reaction region. The conservation in the reaction region is then balanced between the diffusion and reaction processes. Convection transport is less important in the reaction region because the reaction region is thin and it takes a larger length scale to exhibit its variations.

3.5 Formulation of Local Coupling Functions

The equations governing the conservation of reactant concentrations can be derived without including the nonlinear reaction term by the use of local coupling

functions. A coupling function is defined by combining multiple equations to eliminate the reaction term.

In this problem, two coupling functions can be defined. The first is obtained by adding Equations (2.22) and (2.23) together as:

$$\frac{1}{\tilde{r}^2}\frac{d}{d\tilde{r}}\left(\tilde{m}\tilde{T}-\tilde{r}^2\frac{d\tilde{T}}{d\tilde{r}}\right)+\frac{1}{\tilde{r}^2}\frac{d}{d\tilde{r}}\left(\tilde{m}\tilde{Y}_1-\frac{\tilde{r}^2}{Le_1}\frac{d\tilde{Y}_1}{d\tilde{r}}\right)=0 \tag{3.27}$$

This coupling function represents the conservation of total enthalpy, which includes the thermal and chemical enthalpies. Two source-free conservation equations can be derived by substituting Equations (3.18), (3.19), and (3.20) into Equation (3.27), expanding the terms, and keeping the two leading orders in. Only two diffusion terms exist in the leading order equation, which can be integrated once easily to yield:

$$c_1=\frac{d\theta_1}{d\zeta}-\frac{1}{Le_1}\frac{d\phi_1}{d\zeta}=\frac{d}{d\zeta}\left(\theta_1-\frac{\phi_1}{Le_1}\right) \tag{3.28}$$

Equation (3.28) can be integrated again to:

$$c_1\zeta+c_2=\theta_1-\frac{\phi_1}{Le_1} \tag{3.29}$$

Next, the second highest order terms can be grouped and integrated once to:

$$c_3-2c_1\zeta=\left(\frac{d\theta_2}{d\zeta}-\frac{1}{Le_1}\frac{d\phi_2}{d\zeta}\right)+\tilde{m}\left(\phi_1-\theta_1\right) \tag{3.30}$$

The rest of the terms in the expansion are less important in the analysis and will be ignored.

The second coupling function is obtained by subtracting Equation (2.24) from Equation (2.23) to yield:

$$\frac{1}{\tilde{r}^2}\frac{d}{d\tilde{r}}\left(\tilde{m}\tilde{Y}_1-\frac{\tilde{r}^2}{Le_1}\frac{d\tilde{Y}_1}{d\tilde{r}}\right)-\frac{1}{\tilde{r}^2}\frac{d}{d\tilde{r}}\left(\tilde{m}\tilde{Y}_2-\frac{\tilde{r}^2}{Le_2}\frac{d\tilde{Y}_2}{d\tilde{r}}\right)=0 \tag{3.31}$$

This coupling function represents the relation between the reactants. Substituting Equation (3.18), (3.20), and (3.21) into the coupling function, expanding the equation, keeping the two leading order terms in, and integrating the results similar to the procedure used for the first coupling function, yields:

$$c_4=-\frac{1}{Le_1}\frac{d\phi_1}{d\zeta}+\frac{1}{Le_2}\frac{d\psi_1}{d\zeta} \tag{3.32}$$

$$c_4\zeta+c_5=-\frac{\phi_1}{Le_1}+\frac{\psi_1}{Le_2} \tag{3.33}$$

$$c_6-2c_4\zeta=-\frac{1}{Le_1}\frac{d\phi_2}{d\zeta}+\frac{1}{Le_2}\frac{d\psi_2}{d\zeta}+\tilde{m}\left(\phi_1-\psi_1\right) \tag{3.34}$$

3.6 Matching the Outer Solutions with the Solutions in the Reaction Region

Part of the unknown constants in Equations (3.12) – (3.17) and (3.29) – (3.34) can be determined by matching the outer solutions with the solutions in the reaction region. Matching can be performed by understanding that the solutions in these regions must approach each other in a common region between them. This common region is located at $\tilde{r}\to 1$ and $\zeta\to\infty$. Following this concept, matching of the solutions for temperature is through the relation:

$$[\tilde{T}_0^+ +\varepsilon\tilde{T}_1^+ +O(\varepsilon^2)]_{\tilde{r}=1+\varepsilon\zeta}=[\tilde{T}_f-\varepsilon\theta_1-\varepsilon^2\theta_2+O(\varepsilon^3)]_{\xi\to\infty} \tag{3.35}$$

By linearizing the outer solutions through the use of $\tilde{r}=1+\varepsilon\zeta$, rearranging the expression in orders of ε and equating the result with the inner expansion as shown in Equation (3.35), $a_{T,0}^{+}$ is determined in terms of $\tilde{T}_f$ as:

$$a_{T,0}^{+}=\frac{\tilde{T}_f-\tilde{T}_\infty}{1-\exp(-\tilde{m})} \tag{3.36}$$

The matching also provides two conditions as $\zeta\to\infty$, denoted by a superscript "∞", given by:

$$\theta_1^{\infty}=a_{T,1}^{+}[1-\exp(-\tilde{m})]+\tilde{m}\frac{\tilde{T}_f-\tilde{T}_\infty}{1-\exp(-\tilde{m})}\exp(-\tilde{m})\zeta \quad , \tag{3.37}$$

$$\frac{d\theta_2^{\infty}}{d\zeta}-\tilde{m}\theta_1^{\infty}=-\tilde{m}a_{T,1}^{+}-2\tilde{m}a_{T,0}^{+}\exp(-\tilde{m})\zeta \tag{3.38}$$

Similarly, matching of the solutions for the reactants yields:

$$a_{1,0}^{+}=0 \quad , \tag{3.39}$$

$$a_{2,0}^{+}=\frac{\tilde{Y}_{2,\infty}-\psi_0}{[1-\exp(-\tilde{m}Le_2)]} \quad , \tag{3.40}$$

$$\phi_1^{\infty}=a_{1,1}^{+}[1-\exp(-\tilde{m}Le_1)] \quad , \tag{3.41}$$

$$\frac{d\phi_2^{\infty}}{d\zeta}=-\tilde{m}Le_1a_{1,1}^{+}\exp(-\tilde{m}Le_1) \quad , \tag{3.42}$$

$$\frac{d\psi_0}{d\zeta}=0 \quad , \tag{3.43}$$

$$\psi_1^{\infty}=\tilde{m}Le_2a_{2,0}^{+}\exp(-\tilde{m}Le_2)\zeta-a_{2,1}^{+}[1-\exp(-\tilde{m}Le_2)] \quad , \tag{3.44}$$

$$\frac{d\psi_2^{\infty}}{d\zeta} = \tilde{m}Le_2 a_{2,1}^{+} \exp(-\tilde{m}Le_2) + a_{2,0}^{+}\tilde{m}^2 Le_2^2 \exp(-\tilde{m}Le_2)\zeta$$

$$- 2a_{2,0}^{+}\tilde{m}Le_2 \exp(-\tilde{m}Le_2)\zeta \tag{3.45}$$

Equations (3.41) and (3.42) can be rearranged to:

$$\tilde{m}\phi_1^{\infty} - \frac{1}{Le_1}\frac{d\phi_2^{\infty}}{d\zeta} = \tilde{m}a_{1,1}^{+} \tag{3.46}$$

and Equations (3.44) and (3.45) can be re-expressed by:

$$\tilde{m}\psi_1^{\infty} - \frac{1}{Le_2}\frac{d\psi_2^{\infty}}{d\zeta} = -ma_{2,1}^{+} + 2a_{2,0}^{+}\tilde{m}\exp(-\tilde{m}Le_2)\zeta \tag{3.47}$$

3.7 Boundary Conditions at the Burner Surface

The remaining unknowns need to be determined through the application of the boundary conditions at the burner exit, shown in Equation (2.27a – d). Because the burner is attached to the reaction region, these boundary conditions are applicable to the solutions in the reaction region. When the flame first reaches the burner, the burner is located at $\tilde{r}=1$ with $\zeta \to -\infty$ as for typical diffusion flames. With a further reduction of the mass flow rate, the flame continues to move towards the burner such that the burner is located at a finite position given by $\zeta=-\zeta_b$. Expanding $\tilde{T}_b$ to:

$$\tilde{T}_b = \tilde{T}_{b,0} + \varepsilon\tilde{T}_{b,1} + \varepsilon^2\tilde{T}_{b,2} + O(\varepsilon^3) \tag{3.48}$$

and equating Equation (3.19) with (3.48) at $\zeta=-\zeta_b$, we obtain $\tilde{T}_f = \tilde{T}_{b,0}$, as should be because the flame is attached to the burner exit, and

$$\theta_1(\zeta = -\zeta_b) = \tilde{T}_{b,1} \quad , \tag{3.49}$$

$$\theta_2(\zeta = -\zeta_b) = \tilde{T}_{b,2} \tag{3.50}$$

Next applying Equations (3.6) and (3.19) to Equation (2.27b) at $\tilde{r}$=1 and ζ=$-\zeta_b$ yields:

$$\left(\frac{d\theta_1}{d\zeta}\right)_{-\zeta_b} = -\tilde{m}(\tilde{T}_f - \tilde{T}_0) \quad , \tag{3.51}$$

$$\left(\frac{d\theta_2}{d\zeta}\right)_{-\zeta_b} = \tilde{m}\tilde{T}_{b,1} \tag{3.52}$$

Equations (3.49) and (3.52) can be combined to:

$$\left(\frac{d\theta_2}{d\zeta}\right)_{-\zeta_b} - \tilde{m}\theta_1(\zeta = -\zeta_b) = 0 \tag{3.53}$$

Similarly, substitution of Equations (3.20) and (3.21) to Equations (2.27c) and (2.27d), respectively, yields:

$$\left(\frac{d\phi_1}{d\zeta}\right)_{\zeta=-\zeta_b} = -\tilde{m}Le_1 \quad , \tag{3.54}$$

$$\frac{1}{Le_1}\left(\frac{d\phi_2}{d\zeta}\right)_{-\zeta_b} - \tilde{m}\phi_1(\zeta=-\zeta_b)=0 \quad , \tag{3.55}$$

$$\left(\frac{d\psi_1}{d\zeta}\right)_{\zeta=-\zeta_b} = \tilde{m}Le_2\{\tilde{Y}_{2,\infty} - a^+_{2,0}[1-\exp(-\tilde{m}Le_2)]\} \quad , \tag{3.56}$$

$$\frac{1}{Le_2}\left(\frac{d\psi_2}{d\zeta}\right)_{-\zeta_b} - \tilde{m}\psi_1(\zeta=-\zeta_b)=0 \tag{3.57}$$

3.8 Solutions of the Equations in the Reaction Region

The inner equations can now be solved subject to the boundary conditions at ζ=$-\zeta_b$ and $\zeta\to\infty$. To begin with, c_1 can be determined by substituting the

differentiation of Equations (3.37) and (3.41) into Equation (3.28), as well as substituting Equations (3.51) and (3.54) into Equation (3.28). Comparison of the two expressions for c_1 results in the solutions of $\tilde{T}_f$ and $a^+_{T,0}$, given by:

$$\tilde{T}_f = \tilde{T}_b = 1 + \tilde{T}_0 - (1 + \tilde{T}_0 - \tilde{T}_\infty)\exp(-\tilde{m}) \quad , \tag{3.58}$$

$$a^+_{T,0} = (1 + \widetilde{T}_0 - \widetilde{T}_\infty) \tag{3.59}$$

As an extension, substitution of Equations (3.37) and (3.41), as well as Equation (3.49), into Equation (3.29) gives:

$$\phi_1(-\zeta_b) = Le_1[\tilde{m}(1 + \widetilde{T}_0 - \widetilde{T}_\infty)\exp(-\tilde{m})\zeta_b] + a^+_{1,1}[1 - \exp(-\tilde{m}Le_1)] \tag{3.60}$$

Next, substituting Equations (3.38) and (3.46), as well as Equations (3.49), (3.53) and (3.55), into Equation (3.30) gives another relation:

$$a^+_{1,1} - a^+_{T,1} = -2(1 + \widetilde{T}_0 - \widetilde{T}_\infty)\exp(-\tilde{m})\zeta_b \tag{3.61}$$

Following the same procedure and applying the appropriate conditions at $\zeta = -\zeta_b$ and $\zeta \to \infty$, Equations (3.42) and (3.45), as well as the derivatives of Equation (3.44) and (3.41), are substituted into Equation (3.32) – (3.34) to yield:

$$a^+_{2,0} = 1 + \widetilde{Y}_{2,\infty} \quad , \tag{3.62}$$

$$\psi_0 = \widetilde{Y}_{2,\infty} - (1 + \widetilde{Y}_{2,\infty})[1 - \exp(-\tilde{m}Le_2)] = (1 + \widetilde{Y}_{2,\infty})\exp(-\tilde{m}Le_2) - 1 \quad , \tag{3.63}$$

$$\psi_1(-\zeta_b) = Le_2\{\tilde{m}[(1 + \widetilde{T}_0 - \widetilde{T}_\infty)\exp(-\tilde{m}) - (1 + \widetilde{Y}_{2,\infty})\exp(-\tilde{m}Le_2)]\zeta_b\} - a^+_{2,1}[1 - \exp(-\tilde{m}Le_2)] \quad , \tag{3.64}$$

$$a^+_{1,1} + a^+_{2,1} = -2a^+_{2,0}\exp(-\tilde{m}Le_2)\zeta_b = -2(1 + \widetilde{Y}_{2,\infty})\exp(-\tilde{m}Le_2)\zeta_b \tag{3.65}$$

For simplicity in the numerical integration of Equation (3.25), a coordinate transformation using $\hat{\zeta}$ as the spatial coordinate where:

$$\hat{\zeta} = \zeta + \zeta_b \tag{3.66}$$

is introduced. In this new coordinate, the burner exit is located at $\hat{\zeta}=0$. Applying this transformation, Equations (3.25), (3.37), (3.49) and (3.51) are transformed to:

$$d^2\theta_1 / d\zeta^2 = \Lambda\{Le_1[\theta_1 + A_T - \tilde{m}(1+\tilde{T}_0 - \tilde{T}_\infty)\exp(-\tilde{m})\hat{\zeta}]$$

$$+ a^+_{1,1}[1-\exp(-\tilde{m}Le_1)]\}\exp(-\theta_1) \tag{3.67}$$

$$\hat{\zeta} = 0 \quad , \quad \theta_1 = \tilde{T}_{b,1} \quad , \quad \left(\frac{d\theta_1}{d\hat{\zeta}}\right) = -\tilde{m}(\tilde{T}_f - \tilde{T}_0) \tag{3.68}$$

$$\hat{\zeta} \to \infty \quad , \quad \theta_1^\infty = A_T - \tilde{m}(1+\tilde{T}_0 - \tilde{T}_\infty)\exp(-\tilde{m})\hat{\zeta} \tag{3.69}$$

$$d\theta_1^\infty / d\hat{\zeta} = -\tilde{m}(1+\tilde{T}_0 - \tilde{T}_\infty)\exp(-\tilde{m}) \tag{3.70}$$

where A_T is expressed by:

$$A_T = -a^+_{T,1}[1-\exp(-\tilde{m})] + \tilde{m}(1+\tilde{T}_0 - \tilde{T}_\infty)\exp(-\tilde{m})\zeta_b \tag{3.71}$$

and the reduced Damköhler number, Λ, is updated to:

$$\Lambda = \varepsilon^2 Da[(1+\tilde{Y}_{2,\infty})\exp(-\tilde{m}Le_2) - 1]\exp\{-\tilde{E}/[1+\tilde{T}_0 - (1$$

$$+ \tilde{T}_0 - \tilde{T}_\infty)\exp(-\tilde{m})]\} \tag{3.72}$$

3.9 Solutions for Flame Temperature and Flame Location for a Detached Flame in the Reaction-Sheet Limit

The analysis is completed at this stage. All the unknowns have been determined either explicitly or can be determined through the numerical integration of Equation (3.67) subject to Equations (3.68), (3.69) and (3.70). There are, however, two important quantities still missing, namely the adiabatic flame temperature of the flame and the maximum flow rate above which the flame is detached from the burner. These solutions can be obtained from the analysis of the detached flame in the reaction sheet limit. As discussed earlier, in the reaction sheet limit, combustion reaction occurs only on an infinitely thin flame sheet. There are two preheat regions that sandwich the flame sheet. On the flame sheet located at $\tilde{r}=\tilde{r}_f$, all the reactants are consumed such that the conditions are:

$$\tilde{r}=\tilde{r}_f: \quad \tilde{T}=\tilde{T}_f \quad , \quad \tilde{Y}_1=\tilde{Y}_2=0 \tag{3.73}$$

In the transport region between the burner and the flame sheet, bounded by $1<\tilde{r}<\tilde{r}_f$, $\tilde{Y}_2^- \equiv 0$ because all the ambient reactant is consumed at the flame sheet. The solutions of $\tilde{T}$ and $\tilde{Y}_1$ can be obtained by integrating the source-free expressions of Equations (2.22) and (2.23) subject to Equaions (2.27a – c) and (3.e), and the derivative of Equation (3.6) to yield:

$$\widetilde{T}^- = \widetilde{T}_0 + (\widetilde{T}_f - \widetilde{T}_0)\exp[\widetilde{m}(\widetilde{r}_f^{-1} - \widetilde{r}^{-1})] \quad , \tag{3.74}$$

$$\widetilde{Y}_1^- = 1 - \exp[\widetilde{m}Le_1(\widetilde{r}_f^{-1} - \widetilde{r}^{-1})] \quad , \tag{3.75}$$

In the transport region outside of the flame sheet, $\tilde{r}_f < \tilde{r} < \infty$, the solutions of $\tilde{T}$ and $\tilde{Y}_2$ are determined by integrating the source-free expressions of Equations (2.22) and (2.24) subject to Equaions (2.28) and (3.73) to yield:

$$\widetilde{T}^{+} = \widetilde{T}_{\infty} - (\widetilde{T}_{\infty} - \widetilde{T}_{f}) \frac{1 - \exp(-\widetilde{m}/\widetilde{r})}{1 - \exp(-\widetilde{m}/\widetilde{r}_{f})} \tag{3.76}$$

$$\widetilde{Y}_{2}^{+} = \widetilde{Y}_{2,\infty} \frac{\exp(-\widetilde{m} Le_2/\widetilde{r}) - \exp(-\widetilde{m} Le_2/\widetilde{r}_{f})}{1 - \exp(-\widetilde{m} Le_2/\widetilde{r}_{f})} \tag{3.77}$$

In the above, superscripts "–" and "+" denote, respectively, the solutions between the burner and the flame sheet, and outside of the flame sheet.

Integrating the coupling function shown in Equation (3.27) across the flame sheet and applying Equation (3.73), a jump condition is obtained,

$$\left(\frac{d\tilde{T}^{+}}{d\tilde{r}}\right)_{\tilde{r}_f} = \left(\frac{d\tilde{T}^{-}}{d\tilde{r}}\right)_{\tilde{r}_f} + \frac{1}{Le_1}\left(\frac{d\tilde{Y}_1^{-}}{d\tilde{r}}\right)_{\tilde{r}_f} \tag{3.78}$$

The flame temperature is solved by substituting Equations (3.74) – (3.75) into Equation (3.78) to yield:

$$\widetilde{T}_f = 1 + \widetilde{T}_0 - [1 + \widetilde{T}_0 - \widetilde{T}_{\infty}] \exp(-\widetilde{m}/\widetilde{r}_f) \tag{3.79}$$

Similarly, integrating the coupling function of Equation (3.31) across the flame sheet gives the jump condition

$$\frac{1}{Le_1}\left(\frac{d\tilde{Y}_1^{-}}{d\tilde{r}}\right)_{\tilde{r}_f} + \frac{1}{Le_2}\left(\frac{d\tilde{Y}_2^{+}}{d\tilde{r}}\right)_{\tilde{r}_f} = 0 \tag{3.80}$$

Substitution of Equations (3.75) and (3.77) into Equation (3.80) then provides the flame location, given by:

$$\tilde{r}_f = \frac{\tilde{m} Le_2}{\ln(1+\tilde{Y}_{2,\infty})} \tag{3.81}$$

Equation (3.81) reveals that the flame location is independent of the Lewis number of the burner reactant. This is because all the reactants supplied from the burner are completely consumed regardless of diffusion rate. When the diffusion rate of the ambient reactant is increased (Le_2 is decreased), the reactant is transported to the flame at a higher rate. As a result, the flame shifts towards the burner direction to seek for a larger amount of the burner reactant and $\tilde{r}_f$ is reduced.

Application of Equation (3.81) to (3.79) yields an alternative expression for the flame temperature, given by:

$$\tilde{T}_f = 1 + \tilde{T}_0 - \frac{1 + \tilde{T}_0 - \tilde{T}_\infty}{(1+\tilde{Y}_{2,\infty})^{1/Le_2}} \tag{3.82}$$

which depends only on the specified flow conditions. The adiabatic flame temperature is the value of $\tilde{T}_f$ when $Le_2 = 1$, and is expressed as:

$$\tilde{T}_{ad} = 1 + \tilde{T}_0 - \frac{1 + \tilde{T}_0 - \tilde{T}_\infty}{1+\tilde{Y}_{2,\infty}} \tag{3.83}$$

The maximum mass flow rate can be identified from Equation (3.81) by setting $\tilde{r}_f = 1$ as:

$$\tilde{m} = \frac{\ln(1+\tilde{Y}_{2,\infty})}{Le_2} \tag{3.84}$$

This work focuses on flames with mass flows lower than the flow rate given by Equation (3.84).

3.10 Rescaling

Since the values of nondimensionalization parameters are different for different representative flames, the results could be misleading when comparing the results of the four limiting flames mentioned in Chapter 1. To avoid any misconceptions, the parameters are rescaled to be independent of flow conditions and flame type. As an example, the temperatures are rescaled by using the heat of combustion per unit mass of the fuel, q_f, instead of q_1 such that:

$$\overline{T} = \frac{c_p T}{q_F} \tag{3.85}$$

Applying Equation (3.85), the adiabatic flame temperature is rescaled to:

$$\overline{T}_{ad} = \frac{q_1 Y_{1,0}}{q_F} + \overline{T}_0 - \frac{\frac{q_1 Y_{1,0}}{q_F} + \overline{T}_0 - \overline{T}_\infty}{1 + \widetilde{Y}_{2,\infty}} \tag{3.86}$$

and the activation temperature is rescaled to:

$$\overline{E} = \frac{c_p E}{q_F} \tag{3.87}$$

Similarly, the mass flow rate is rescaled to:

$$\overline{m} = \frac{c_p m}{4\pi r_b^* \lambda_g} \tag{3.88}$$

such that the mass flow rate for an attached flame is bounded by:

$$\overline{m} \le \frac{1}{Le_2} \frac{r_b}{r_b^*} \frac{m_F}{m} \ln(1 + \widetilde{Y}_{2,\infty}) \tag{3.89}$$

Applying the rescaled nondimensional quantities, the relevant parameters are modified to:

$$\overline{Da} = \frac{\nu_F W_F c_p r_b^{*2} B \rho_{ad}^2}{\lambda_g} \tag{3.90}$$

$$\bar{\varepsilon} = \overline{T}_{ad}{}^2 / \overline{E} \tag{3.91}$$

$$\overline{\Lambda} = \bar{\varepsilon}^2 \overline{Da} \exp(-\overline{E} / \overline{T}_{ad}) \tag{3.92}$$

such that

$$Da = \frac{\nu_2 W_2}{\nu_F W_F} \frac{r_b^2}{r_b^{*2}} Y_{1,0} \frac{\overline{T}_{ad}^2}{\overline{T}_f^2} \overline{Da} \tag{3.93}$$

$$\varepsilon = \frac{q_F}{q_1 Y_{1,0}} \frac{\overline{T}_f^2}{\overline{T}_{ad}^2} \bar{\varepsilon} \tag{3.94}$$

$$\Lambda = \left(\frac{q_F}{q_1 Y_{1,0}} \right)^2 \frac{\overline{T}_f^2}{\overline{T}_{ad}^2} \frac{\nu_2 W_2}{\nu_F W_F} \frac{r_b^2}{r_b^{*2}} Y_{1,0} [(1 + \widetilde{Y}_{2,\infty}) \exp(-\tilde{m} Le_2) - 1] \overline{\Lambda} \tag{3.95}$$

$$\bar{a}_{T,1} = (\varepsilon / \bar{\varepsilon}) a_{T,1} \tag{3.96}$$

$$\bar{a}_{1,1} = (\varepsilon / \bar{\varepsilon}) a_{1,1} \tag{3.97}$$

CHAPTER 4

RESULTS AND DISCUSSION

4.1 Numerical Approach

The analysis presented in Chapter 3 reduces the equations to a nonlinear second order differential equation, Equation (3.67), which needs to be integrated numerically. To exhibit the feature of the results, sample calculations are performed to solve for the flame temperature, reactant leakage, and extinction condition, iteratively. The thermal physical values used are given by:

$$T_0 = 298K \quad , \quad T_\infty = 298K \quad , \quad E = 24000K \quad ,$$

$$q_F = 47160\ J/g \quad , \quad c_{p,g} = 1.32320\ J/(g.K) \quad , \quad \lambda_g = 0.00120430\ W/(cm.K) \quad ,$$

$$r_{b,R} = 0.3175\ cm \quad , \quad r_b = 0.3175\ cm \quad ,$$

$$\nu_F = 1.00 \quad , \quad \nu_O = 3.00 \quad , \quad W_F = 28\ g/mole \quad , \quad W_O = 32\ g/mole$$

These values mimic microgravity experiments of ethylene flames burning in air conducted at the NASA Glenn Research Center in the 2.2 second drop tower by Sunderland et al. [30] and [31]. As mentioned in Chapter 1, the flow direction and the amount of inert supply can be independently controlled for the burner-stabilized flame. Taking advantage of this flexibility, four limiting flames that have the same overall mixture composition as the fuel/air flame, similar to those studied by Sunderland et al. [30] and [31], and Liu et al. [32] were considered. The four flames analyzed are (A) fuel issuing into air, (B) diluted fuel issuing into oxygen, (C) air issuing into fuel, and (D) oxygen issuing into diluted fuel. Flame (B) is obtained by extracting the inert gas (e.g., nitrogen) from the air and diverting it to the fuel, and Flames (C) and (D) are inverse of

Flames (A) and (B). The flow direction is from the fuel to the oxidizer for Flames (A) and (B), and from the oxidizer to the fuel for Flames (C) and (D). These flames have the same stoichiometric ratio and adiabatic flame temperature.

A FORTRAN code was created to solve Equation (3.67) subject to the boundary conditions in Equations (3.68), (3.69), and (3.70) by employing a Fourth Order Runge Kutta method. The study starts from the computations performed by keeping the mass flow rate fixed, while varying the kinetic data. Results are presented by plotting the leakage of the reactant supplied from the burner, $\bar{a}_{1,1}$, vs. the reduced Damköhler number, $\overline{\Lambda}$, for selected mass flow rates, as shown in Figures 6, 7, 8, and 9 for Flames (A), (B), (C,) and (D), respectively. The Lewis number of both of the reactants are unity in these computations. It is seen from these figures that for each mass flow rate, there are two solutions corresponding to a value of $\overline{\Lambda}$ when the reaction is sufficiently strong ($\overline{\Lambda}$ is sufficiently large). By decreasing the value of $\overline{\Lambda}$ (weakening the reaction), the two solutions approach each other. There exists a minimum $\overline{\Lambda}$ at which the two solutions merge to one and there is no solution below this critical value. This minimum value of $\overline{\Lambda}$, below which a solution does not exist, represents the slowest reaction rate that a flame can be sustained and is defined as the kinetic extinction limit. The lower branch of the curve, showing a small amount of reactant leakage in the presence of a flame and an increase of reactant leakage with decreasing reaction rate, is the physically realistic solution.

These figures also reveal that for each type of flame, the flame supported by a lower mass flow rate has a larger amount of reactant leakage for the same value of $\overline{\Lambda}$ and is extinguished at a larger value of $\overline{\Lambda}$, meaning that it is easier to be extinguished. This

is realistic because the flame with a smaller flow rate has less burner reactant in the reaction region and has lower flame temperature, as shown in Equation (3.58), similar to the burning of a leaner (with respect to the burner reactant) premixed flame. As is known, the reaction rate of combustion processes is a strong function of the flame temperature because of the high activation energy.

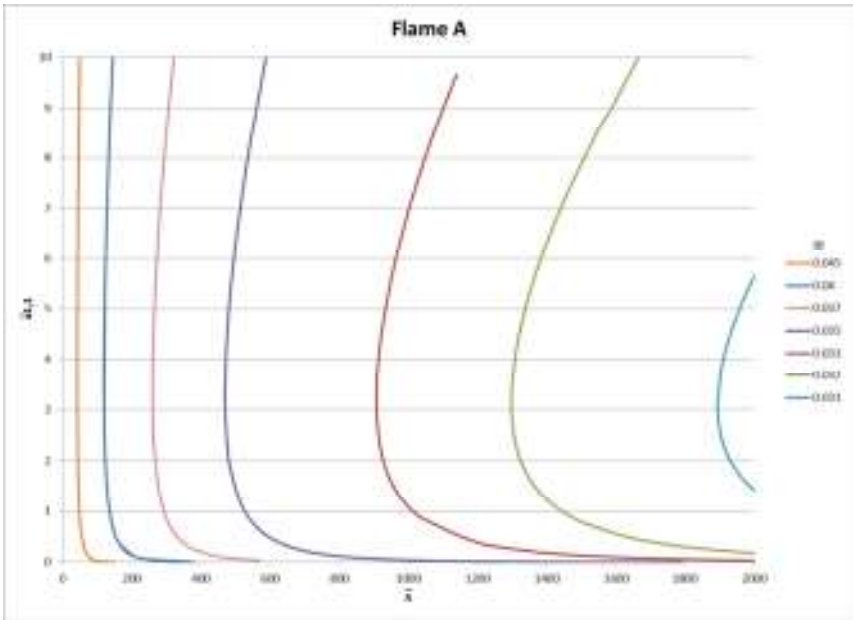

Figure 6. Flame A Reactant Leakage vs. Reduced Damköhler Number for Constant Mass Flow Rates.

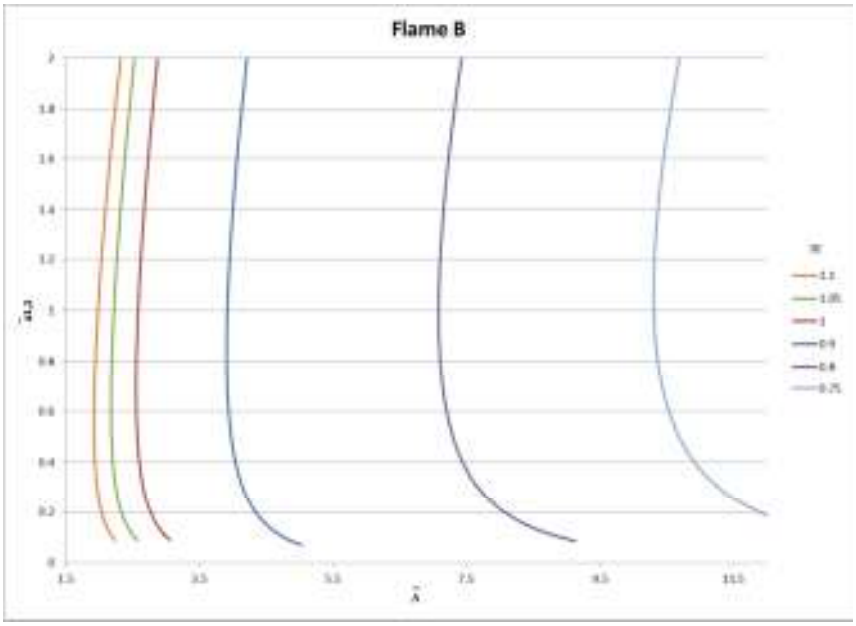

Figure 7. Flame B Reactant Leakage vs. Reduced Damköhler Number for Constant Mass Flow Rates.

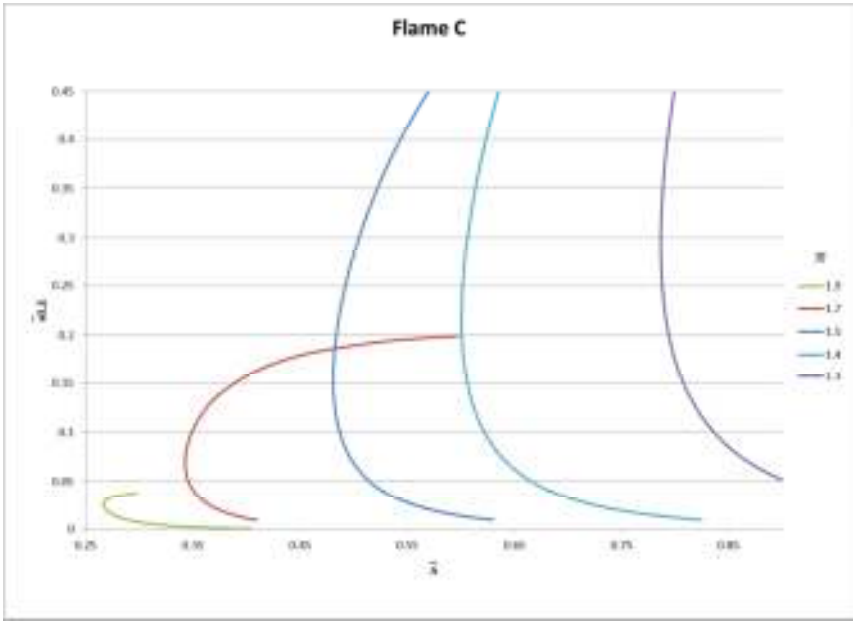

Figure 8. Flame C Reactant Leakage vs. Reduced Damköhler Number for Constant Mass Flow Rates.

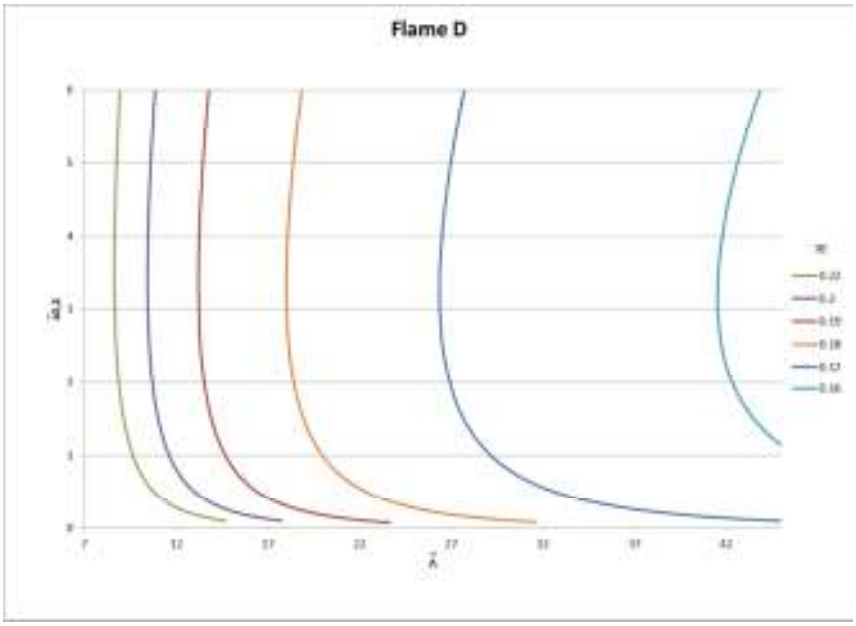

Figure 9. Flame D Reactant Leakage vs. Reduced Damköhler Number for Constant Mass Flow Rates.

While the above discussion is informative in exhibiting the burning and extinction behaviors, it is not physical because it is difficult to vary the kinetic data for a specified mixture. It is more realistic to keep the reduced Damköhler number fixed and vary the flow rate. Figures 10 – 13 plot the reactant leakage versus the mass flow rate for specified values of $\overline{\Lambda}$ for the four limiting flames, similar to those of Figures 6 – 9. The results show that for a given $\overline{\Lambda}$, the reaction is weaker by reducing the mass flow rate, and there exists a minimum mass flow rate below which the flame extinguishes. This is in agreement with the discussion in the previous paragraph.

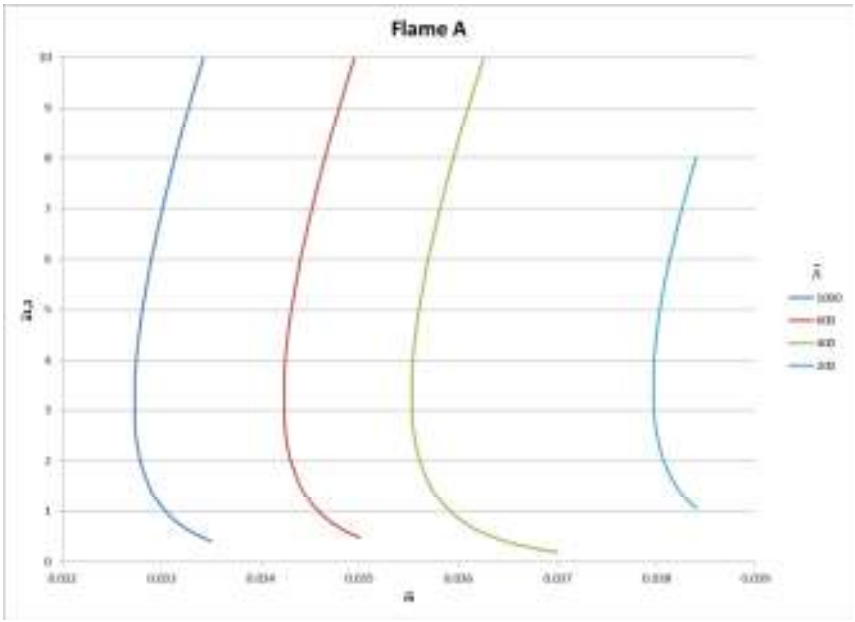

Figure 10. Flame A Reactant Leakage vs. Mass Flow Rate for Constant Reduced Damköhler Number.

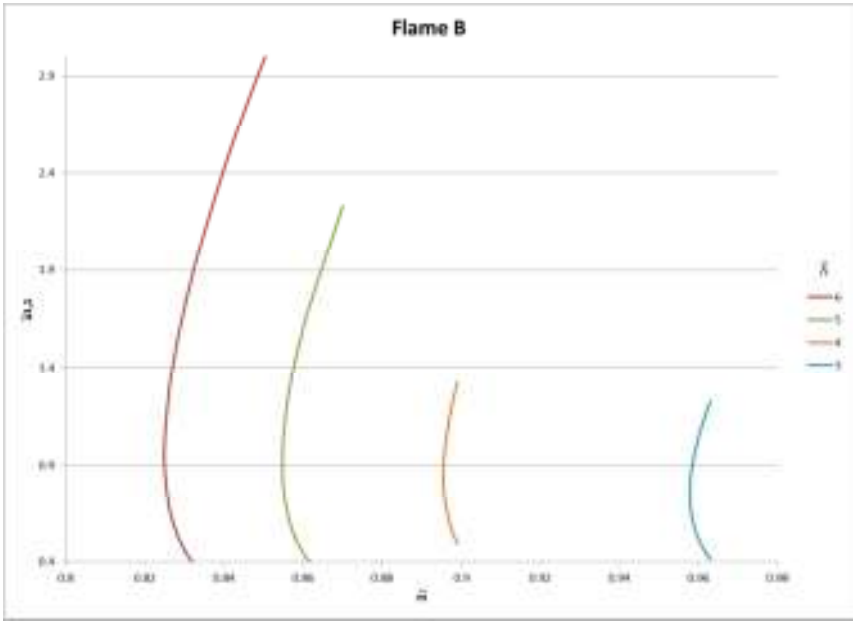

Figure 11. Flame B Reactant Leakage vs. Mass Flow Rate for Constant Reduced Damköhler Number.

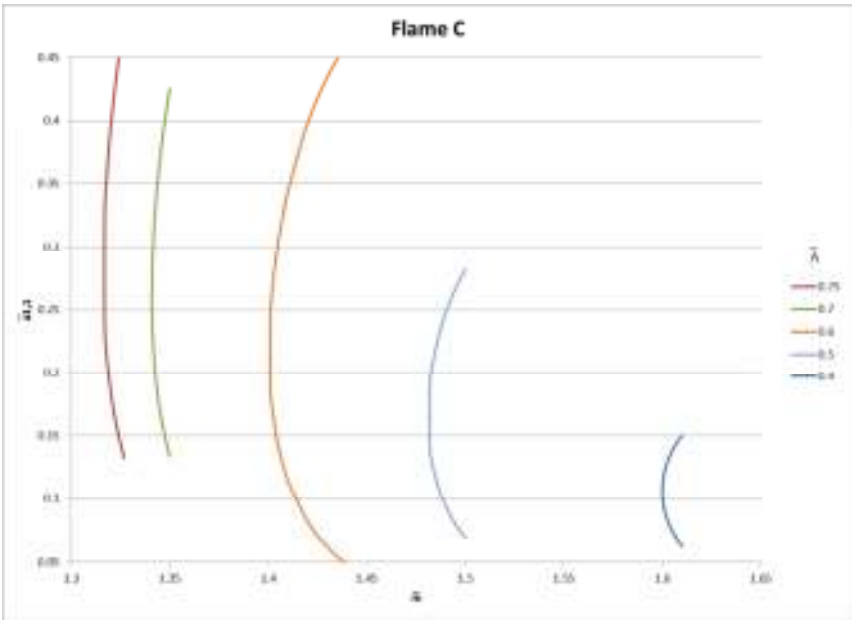

Figure 12. Flame C Reactant Leakage vs. Mass Flow Rate for Constant Reduced Damköhler Number.

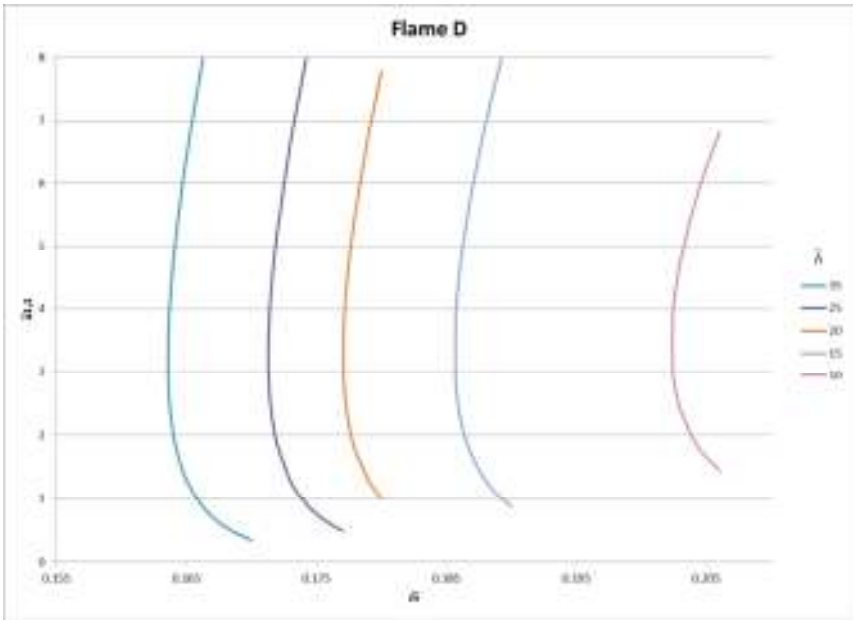

Figure 13. Flame D Reactant Leakage vs. Mass Flow Rate for Constant Reduced Damköhler Number.

The extinction states of the four flames are shown in Figure 14 by plotting the mass flow rate versus the reduced Damköhler number on a logarithmic scale at extinction for the four flames. Comparison of the extinction states exhibit that Flame A is easiest to extinguish, followed by Flames D and B, and Flame C is the strongest flame. For the flames with the same fuel consumption rate, the mass flow rate follows the same sequence, i.e., Flame A has the lowest mass flow rate and Flame C has the highest mass flow rate. When the mass flow rate is increased, a stronger outward convection slows down the transport of the ambient reactant to the reaction region. As a consequence, the reactants in the reaction region are more stoichiometric, the flame temperature is higher, and the flame has a stronger capability to resist extinguishment.

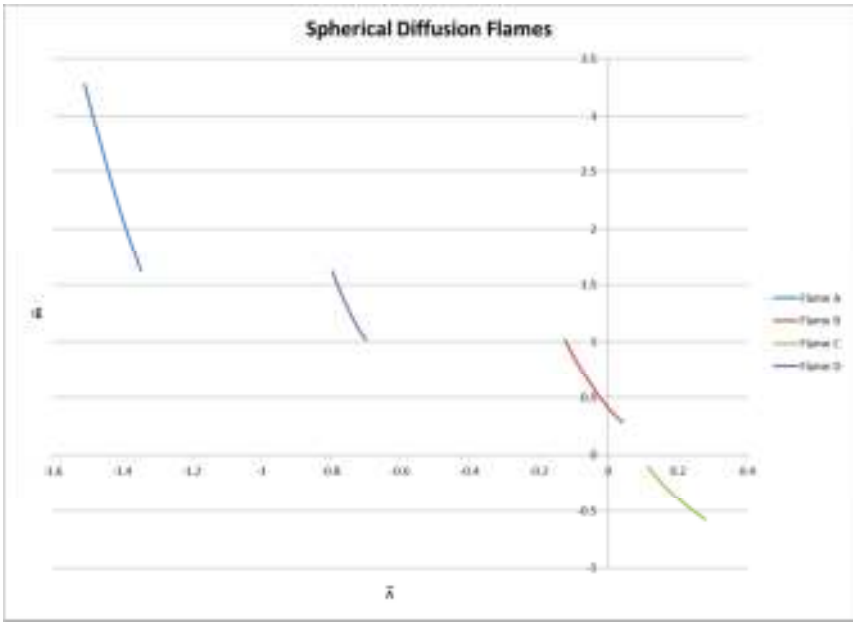

Figure 14. Mass Flow Rate vs. Reduced Damköhler at the Extinction Condition.

The effect of mass diffusion of the ambient species on the flame behavior is shown in Figures 15 – 18 by plotting the leakage of the burner reactant against the mass

flow rate for different Lewis number of the ambient reactant, Le_2, for the four limiting flames. These figures show that the flame is extinguished at smaller flow rate, meaning that the burning intensity is stronger, for lower values of Le_2. This behavior is qualitatively similar for all four flames regardless of the flow direction and inert distribution. As defined earlier, Lewis number is the ratio between the thermal and mass diffusivities. For a fixed thermal diffusivity, the Lewis number is increased when the mass diffusivity is reduced. When Le_2 is decreased, the mass diffusion rate of the ambient reactant is higher and a larger amount of the ambient reactant is transported to the reaction region as shown in Equation (3.63). The existence of additional ambient reaction helps to consume more burner reactant, reduce the leakage of the burner reactant, and delays extinction.

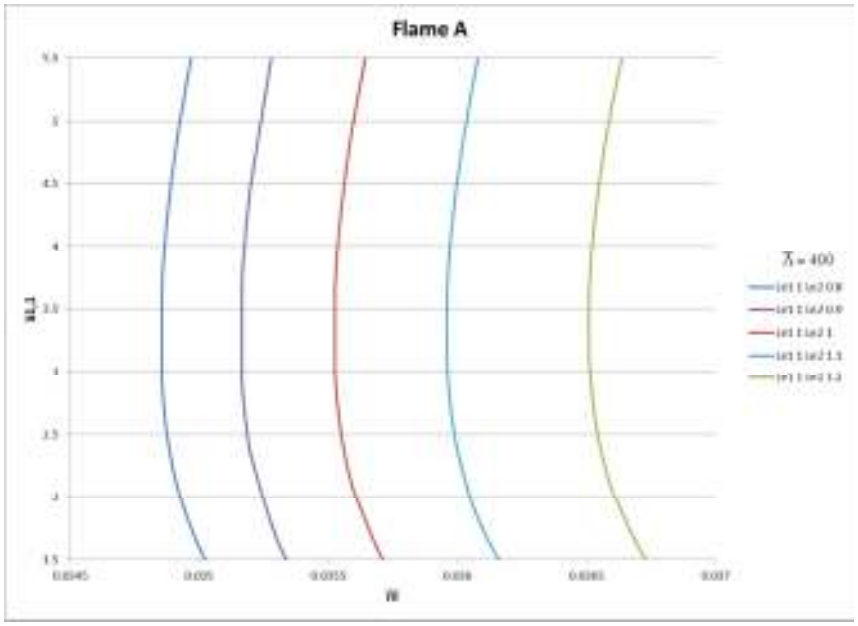

Figure 15. Flame A Reactant Leakage vs. Mass Flow Rate for a Constant Reduced Damköhler Number of 400 and Lewis Number of Burner Reactant at Unity.

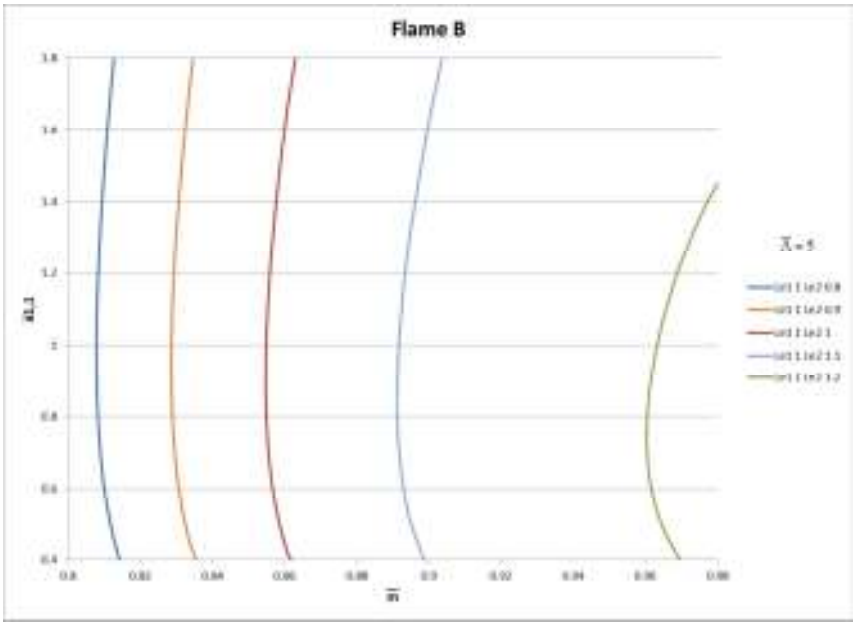

Figure 16. Flame B Reactant Leakage vs. Mass Flow Rate for Constant Reduced Damköhler Number of 5 and Lewis Number of Burner Reactant at Unity.

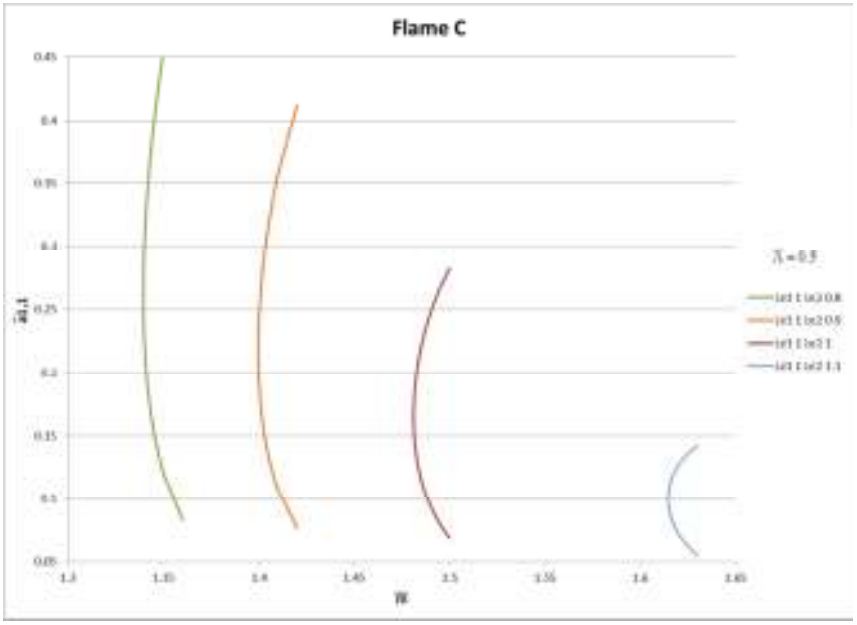

Figure 17. Flame C Reactant Leakage vs. Mass Flow Rate for Constant Reduced Damköhler Number of 0.5 and Lewis Number of Burner Reactant at Unity.

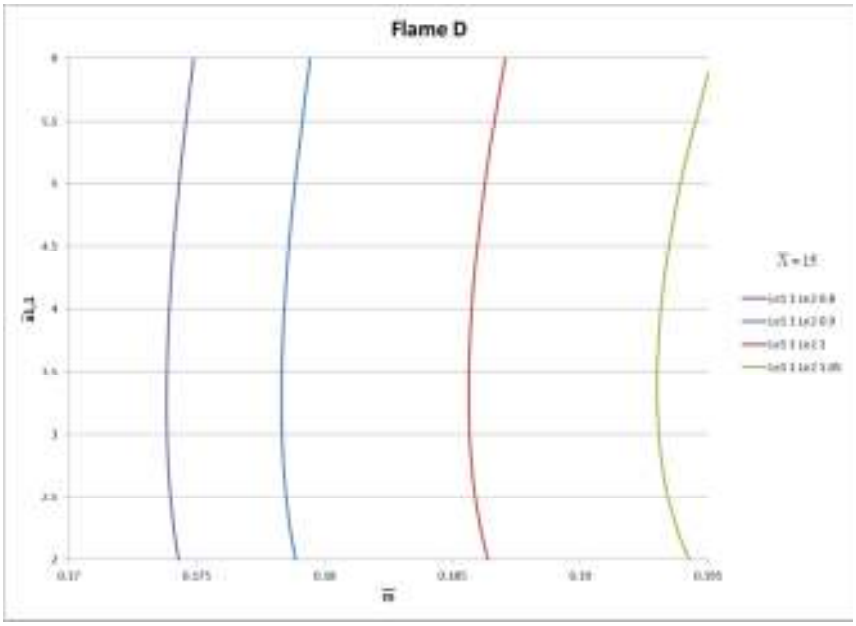

Figure 18. Flame D Reactant Leakage vs. Mass Flow Rate for Constant Reduced Damköhler Number of 15 and Lewis Number of Burner Reactant at Unity.

The effect of mass diffusion of the burner species is also studied and the results are presented in Figures 19 – 22 by plotting the leakage of the burner reactant against the mass flow rate for different Lewis number of the burner reactant, Le_1, for the four limiting flames. Similar to Figures 15 – 18, the result is qualitatively similar for all four flames. However, the effect of Le_1 is reversed from that of Le_2. That is, the flame is extinguished at a smaller flow rate for higher values of Le_1. By decreasing the value of Le_1, the mass diffusion rate of the burner reactant is higher, such that the reactant passes through the reaction region at a higher velocity. As a consequence, more burner reactant escapes from the reaction region without been consumed such that the reactant leakage is increased and the flame becomes weaker. The effect of Le_1 is to modify the residence time of the burner reactant in the reaction region.

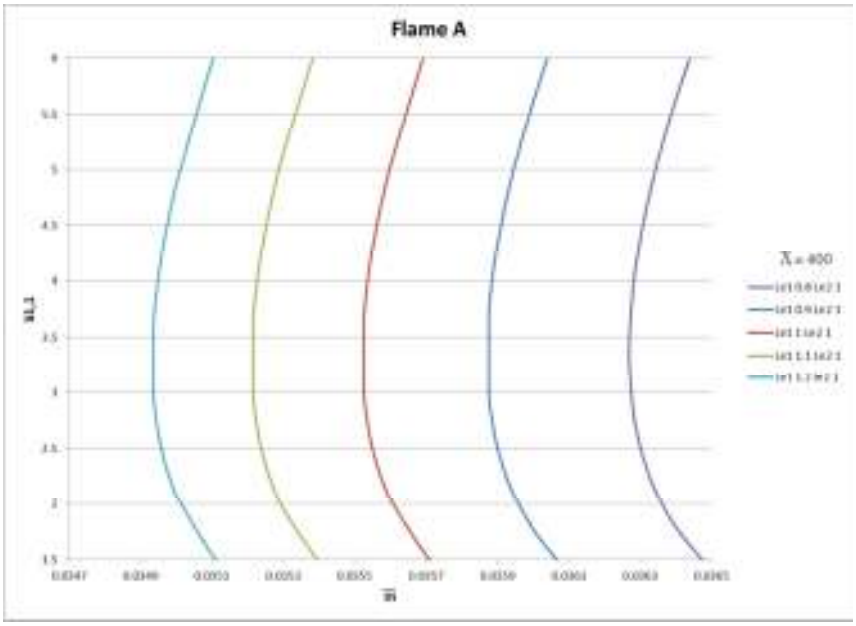

Figure 19. Flame A Reactant Leakage vs. Mass Flow Rate for Constant Reduced Damköhler Number of 400 and Lewis Number of Ambient Reactant at Unity.

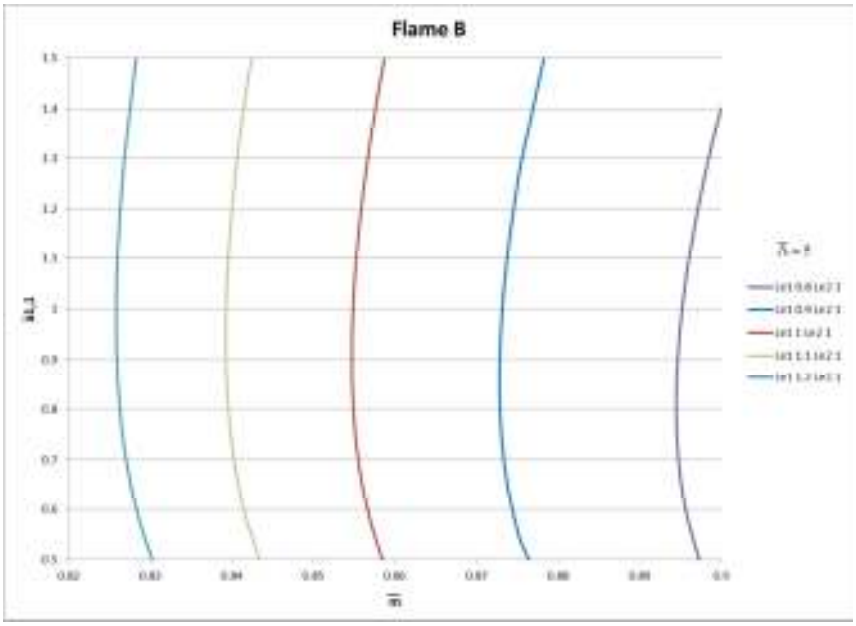

Figure 20. Flame B Reactant Leakage vs. Mass Flow Rate for Constant Reduced Damköhler Number of 5 and Lewis Number of Ambient Reactant at Unity.

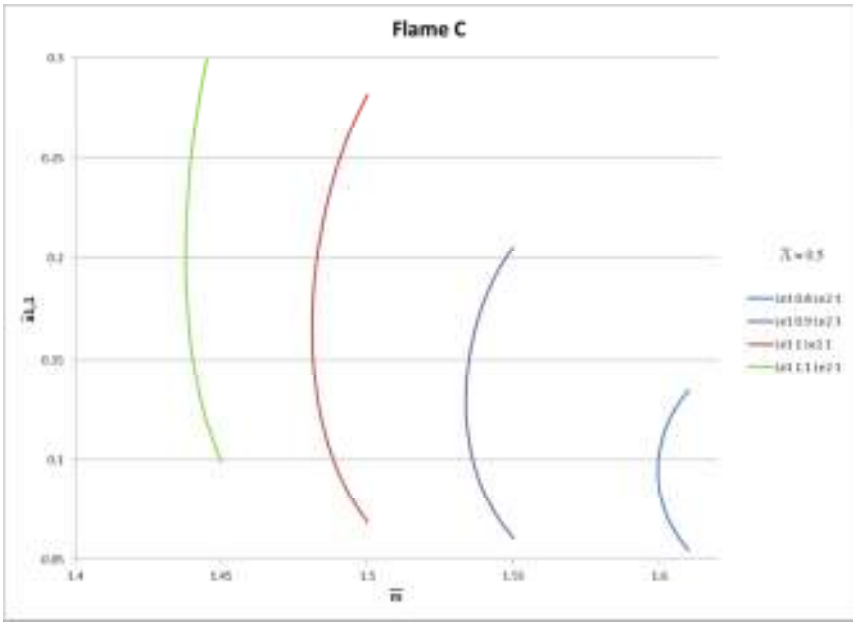

Figure 21. Flame C Reactant Leakage vs. Mass Flow Rate for Constant Reduced Damköhler Number of 0.5 and Lewis Number of Ambient Reactant at Unity.

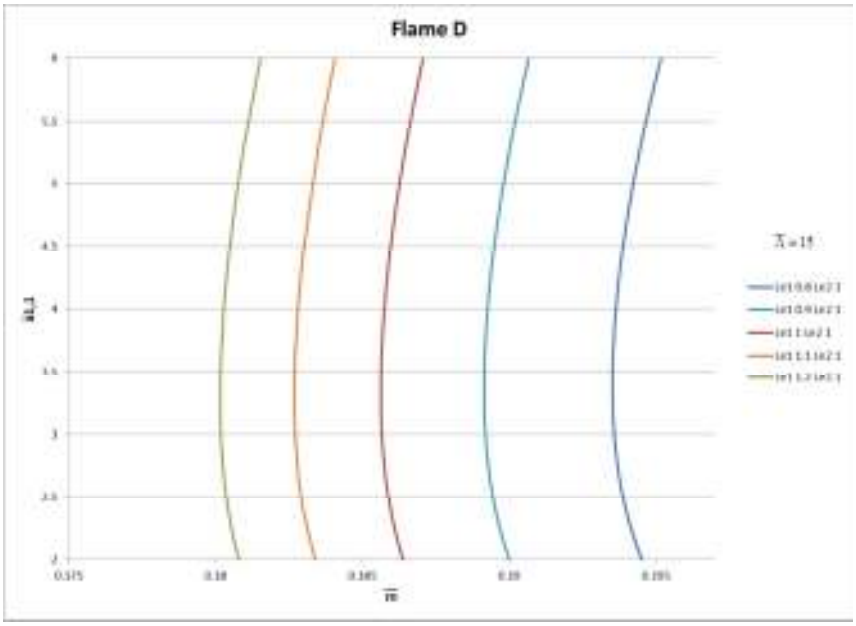

Figure 22. Flame D Reactant Leakage vs. Mass Flow Rate for Constant Reduced Damköhler Number of 15 and Lewis Number of Ambient Reactant at Unity.

The discussion is closed by noting that unlike the detached flame, the leading order flame temperature of the attached flame is independent of the Lewis numbers, as shown in Equation (3.58). This is because the attached flame behaves like a lean premixed flame (referring to the burner reactant) and the flame temperature is determined by the supply of the burner reactant.

CHAPTER 5

CONCLUDING REMARKS AND FUTURE WORKS

In this study, the extinction characteristics of a spherical diffusion flame stabilized by and attached to the exit of a spherical porous burner in microgravity were analyzed using activation energy asymptotics. Four limiting flames having the same adiabatic flame temperature but different inert distribution and flow direction were investigated to understand the effects of reaction rate, flow direction, flame structure, residence time and Lewis number of the reactants on the extinction condition. The flow direction was either from the fuel to the oxidizer by issuing a fuel from the burner, or from the oxidizer to the fuel by injecting oxidizer from the burner, into a quiescent ambient that contains the other reactant. The inert gas, e.g. nitrogen, may be supplied either with oxygen or fuel, which varies the flame structure.

For any of the four limiting flames with constant mass flow rate, the flame having a lower reaction rate (Damköhler number) was easier to extinguish due to slower reaction consumption and heat generation rates. When the reaction rate is fixed, a reduction in the mass flow rate resulted in a weaker flame because of the reduced supply of the burner reactant. There exists a minimum flow rate below which extinction occurs.

Comparing the extinction states of the four flames, Flame A had the lowest mass flow rate and was the easiest flame to extinguish, followed by Flames D and B, while Flame C had the highest mass flow rate and was the strongest flame. This observation signifies that a greater outward convection slowed down the transport of the ambient

reactant to the reaction region, yielding a more stoichiometric flame with a higher flame temperature and stronger reaction.

The effects of mass diffusion were exhibited by varying the Lewis number of the reactants. A decrease of the Lewis number (increase of the mass diffusion rate) of the ambient reactant results in a stronger flame, which is more difficult to be extinguished because there is an increased availability of the ambient reactant to react with the burner reactant. On the contrary, the flame becomes weaker and more vulnerable to extinction when the Lewis number of the burner reactant is reduced. The burner reactant passes through the reaction zone at a faster rate when the diffusion rate is increased such that the residence time is reduced.

A flame attached to the burner can be produced by decreasing the mass flow rate from a detached flame. A further reduction of the flow rate after the flame is attached to the burner results in the presence of a significant amount of the ambient reactant in the reaction zone. Consequently, the burning characteristics is transitioned from the diffusion flame regime to the premixed regime as introduced by Liñán. Continuous reduction of the flow rate reduces the supply of the burner reactant and eventually renders the flame to be extinguished like a lean premixed flame (with respect to the burner reactant). This study demonstrates the possibility of diffusion flames burning in the premixed flame regime, which was believed to be not possible in the past because it is in the unstable middle branch of the S-shaped ignition-extinction curve.

The study may be extended to the reaction for different fuel/oxidizer compositions. The effect of burner size can also be investigated to determine whether there exists a minimum burner size below which the flame cannot be attached to the

burner. Experiments can be performed in the future to verify the results obtained from this research.

REFERENCES

[1] C.K. Law , "Combustion Physics," Cambridge University Press, Cambridge, 2006.

[2] U.S. Energy Information Administration, Washington, D.C., 2011 http://www.eia.gov/energyexplained/index.cfm?page=oil_home

[3] Vaclav Smil, "Energy in World History," University of Manitoba, Westview Press, 1994.

[4] "OPEC Annual Statistical Bulletin 2009," Organization of the Petroleum Exporting Countries, 2010

[5] D.B. Spalding, "A Theory of Inflammability Limits and Flame-Quenching," Proceedings of the Royal Society of London A240 (1957) 83-100

[6] A. Liñán, "The Asymptotic Structure of Counterflow Diffusion Flames for Large Activation Energies," Acta Astronautica 1 (1974) 1007-1039

[7] B.H. Chao, C.K. Law, J.S. T'ien, "Structure and Extinction of Diffusion Flames with Flame Radiation," in Symposium (International) on Combustion 23 (1990) 523–531

[8] M. Matalon, "On Flame Stretch," Combustion Science and Technology 31 (1983) 169-182

[9] S.H. Chung, C.K.Law, "An Invariant Derivation of Flame Stretch," Combustion and Flame 55 (1984) 123-126

[10] F.A. Williams, "Progress in Knowledge of Flamelet Structure and Extinction," Progress in Energy and Combustion Science 26 (2000) 657–682

[11] J.D. Buckmaster, G.S. Ludford, "Theory of Laminar Flames," Cambridge University Press, Cambridge, 1982.

[12] F.A. Williams, “Combustion Theory,” second ed., Benjamin/Cummings Inc., Menlo Park, California, 1985.

[13] K.J. Santa, B.H. Chao, P.B. Sunderland, D.L. Urban, D.P. Stocker, R.L. Axelbaum, “Radiative Extinction of Gaseous Spherical Diffusion Flames in Microgravity,” Combustion and Flame 151 (2007) 665-675

[14] J.S. T’ien, “Diffusion Flame Extinction at Small Stretch Rates: the Mechanism of Radiative Loss,” Combustion and Flame 65 (1986) 31–34

[15] B.H. Chao, C.K. Law, “Asymptotic Theory of Flame Extinction with Surface Radiation,” Combustion and Flame 92 (1993) 1–24

[16] K. Maruta, M. Yoshida, H. Guo, Y. Ju, T. Niioka, “Extinction of Low-Stretched Diffusion Flame in Microgravity,” Combustion and Flame 112 (1998) 181–187

[17] Q. Wang, B.H. Chao, “Kinetic and Radiative Extinctions of Spherical Burner-Stabilized Diffusion Flames,” Combustion and Flame 158 (2011) 1532–1541

[18] K. Mills, M. Matalon, “Extinction of Spherical Diffusion Flames in the Presence of Radiant Loss,” in Symposium (International) on Combustion 27 (1998) 2535–2541

[19] F. Liu, G.J. Smallwood, O.L. Gulder, Y. Ju, “Asymptotic Analysis of Radiative Extinction in Counterflow Diffusion Flames of Nonunity Lewis Numbers,” Combustion and Flame 121 (2000) 275–287

[20] H.Y. Wang, W.H. Chen, C.K. Law, “Extinction of Counterflow Diffusion Flames with Radiative Heat Loss and Nonunity Lewis Numbers,” Combustion and Flame 148 (2007) 100–116

[21] C.K. Law, “Asymptotic Theory for Ignition and Extinction in Droplet Burning.” Combustion and Flame 24 (1975) 89-98

[22] D.L. Dietrich, J.B. Haggard, F.L. Dryer, V. Nayagam, B.D. Shaw, F.A. Williams, "Droplet Combustion Experiments in Spacelab," Proceedings of the Combustion Institute 26 (1996) 1201–1207

[23] B. Nayagam, J.B. Haggard, R.O. Colantonio, A.J. Marchese, F.L. Dryer, B.L. Zhang, F.A. Williams, "N-Heptane Droplet Combustion in Oxygen Helium Mixtures at Atmospheric Pressure," AIAA J. 36 (1998) 1369–1378

[24] S.W. Yoo, E.W. Christiansen, C.K. Law, "Oscillatory Extinction of Spherical Diffusion Flames: Micro-Buoyancy Experiment and Computation," Proceedings of the Combustion Institute 29 (2002) 29–36

[25] S. D. Tse, D. Zhu, C. J. Sung, Y. Ju, C. K. Law, "Microgravity Burner-Generated Spherical Diffusion Flames: Experiment and Computation," Combustion and Flame 125 (2001) 1265–1278

[26] K.J. Santa, Z. Sun, B.H. Chao, P.B. Sunderland, R.L. Axelbaum, D.L. Urban, D.P. Stocker, "Numerical and Experimental Observations of Spherical Diffusion Flames," Combustion Theory and Modeling 11 (2007) 639-652

[27] S. Tang, M.K. Chernovsky, H.G. Im, A. Atreya, "A Computational Study of Spherical Diffusion Flames in Microgravity with Gas Radiation Part I: Model Development and Validation," Combustion and Flame 157 (2010) 118–126

[28] S. Tang, H.G. Im, A. Atreya, "A Computational Study of Spherical Diffusion Flames in Microgravity with Gas Radiation. Part II: Parametric Studies of the Diluent Effects on Flame Extinction," Combustion and Flame 157 (2010) 127–136

[29] V.R. Lecoustre, P.B. Sunderland, B.H. Chao, R.L. Axelbaum, 'Modeled Quenching Limits of Spherical Hydrogen Diffusion Flames," Proceedings of the Combustion Institute 34 (2012), in press

[30] P.B. Sunderland, R.L. Axelbaum, D.L. Urban, B.H. Chao, S. Liu, "Effects of Structure and Hydrodynamics on the Sooting Behavior of Spherical Microgravity Diffusion Flames," Combustion and Flame, 132 (2003) 25–33

[31] P.B. Sunderland, D.L. Urban, D.P. Stocker, B.H. Chao, R.L. Axelbaum, "Sooting Limits of Microgravity Spherical Diffusion Flames in Oxygen-Enriched Air and Diluted Fuel," Combustion Science and Technology, 176 (2004) 2143-2164

[32] S. Liu, B.H. Chao, R.L. Axelbaum, "A Theoretical Study on Soot Inception in Spherical Burner-Stabilized Diffusion Flames," Combustion and Flame, 140 (2005) 1–23